國立交通大學

影像與生醫光電研究所

碩士論文

可撓式光子晶體奈米柱雷射

Flexible Photonic Crystal Nanorods Laser

研 究 生：賴坤廷

指導教授：施閔雄　教授

林俊廷　教授

中　華　民　國　101　年　7　月

可撓式光子晶體奈米柱雷射
Flexible Photonic Crystal Nanorods Laser

研 究 生：賴坤廷　　Student：Kun-Ting Lai

指導教授：施閔雄　　Advisor：Min-Hsiung Shih

林俊廷　　Chun-Ting Lin

國 立 交 通 大 學

影像與生醫光電研究所

碩 士 論 文

A Thesis

Submitted to Institute of Imaging and Biomedical Photonics

College of Photonics

National Chiao Tung University

in partial Fulfillment of the Requirements

for the Degree of

Master

in

Imaging and Biomedical Photonics

July 2012

Tainan, Taiwan, Republic of China

中華民國 101 年 7 月

可撓式光子晶體奈米柱雷射

研究生：賴坤廷

指導教授：施閔雄　教授

林俊廷　教授

摘要

近年來，微觀尺度的光子晶體結構在各種光學應用上已被大量發展，而應用於積體光路上的雷射光源為其中之一門重要課題，藉由微調光子晶體的幾何結構參數，可得到特定的操作波段以及操作模態。然而，一旦光子晶體的結構製作完成，雷射光波長便已決定而難以改變，而另一方面，以軟性有機材料製作的光學元件有較高的應用性以及低成本等優點。於是我們結合了光子晶體的高密度整合特性與軟性材料的應用適應性等優點於我們的光學元件上，在本篇論文當中，我們展現了以磷砷化銦鎵奈米柱製作於聚二甲基矽氧烷基板上的可撓式光子晶體奈米柱雷射。此類磷砷化銦鎵奈米柱包含了四層增益峰值設計於 1.55 微米光通訊波長的量子井結構，並且我們在 1.55 微米波段附近觀察到了位於高對稱 Γ 點上的能帶邊緣型雷射現象。可撓式雷射的優點之一是光學特性可藉由微調結構參數而改變，我們觀察到了經由增加光子晶體晶格的拉升比例，可輕易的控制雷射光波長的位置。當晶格拉升比例由零提升至 8.88 百分比時，我們可以得到大約 26.4 奈米的近似線性紅移現象，大約是每變動一個晶格百分比時即可獲得 3 奈米的波長變化。如此幾何結構可微調的特性指出了可撓性光子晶體雷射在積體光路的應用中可作為高密度整合的可調諧光源。

Flexible Photonic Crystal Nanorods Laser

Student：Kun-Ting Lai

Advisor：Prof. Min-Hsiung Shih

Prof. Chun-Ting Lin

Abstract

In recent years, the micro-scale photonic crystal structures have been developed for a variety of optical applications. One of the important topics is the compact laser light source in the photonic integrated circuit. Specific wavelengths and operation modes for applications could be achieved by fine-tuning the geometry of the photonic crystal structure. However, the lasing wavelength would hard to be altered once the laser structure was fabricated. On the other hand, the organic/polymer based devices have advantages such as application flexibility and low cost. We combine the features of compactness in photonic crystal and flexibility in flexible materials. In this thesis, a flexible photonic crystal nanorods laser was demonstrated with InGaAsP nanorods on a polydimethylsiloxane (PDMS) substrate. The InGaAsP nanorods content 4 quantum wells which are designed for 1.55 μm communication wavelength. The lasing action was observed around 1550nm which is a band-edge emission at high-symmetry Γ-point of photonic crystals. One of advantages of the flexible laser is the fine-tuning of optical properties by manipulating its geometry. In this work, we observed the lasing wavelength can be controlled by increasing photonic crystal lattice extension. The lasing wavelength was linearly red-shift up to 26.4 nm as the lattice extension percentage increased to 8.88 %. The wavelength tuning rate is approximately 3 nm for 1 % lattice extension. Those geometric fine-tuning properties indicate the flexible photonic crystal laser can be applied as a compact tunable light source in photonic crystal integrated circuits.

Acknowledgement

札札實實的兩年時光，終究是順利地為自己曾經跌跌撞撞的學生生涯勉勉強強畫下了句點。對於研究生這個角色，我尚有許多不足與必須加強之處，但也因為有大家各方面的幫助，讓我能踏實的走過這段旅程並留下些許美好的回憶。

在這裡必須先感謝我的論文指導教授施閔雄老師，不管是在研究上、學業上或是生活上的悉心指導與關懷，讓我得以在這短暫的時間完成了這些研究工作與學位。也要感謝功書學長與旻彥學姐，在元件量測部分付出的辛勞及諸多問題的討論與深究，讓我能更深入的了解自己的研究內容。除此之外，感謝湘諭在我 SEM 被停權手足無措之際在 E-beam 上的幫忙，幫我做了很多會 work 的元件，也要感謝怡君在元件模擬的指導建議，程文學長、耀振學長、晉源學長及子庭在研究上的關心與意見，感謝昭瑋、彥中、志祺等等夥伴在這段時間的幫忙與陪伴。

最後要感謝我的家人們，雖然我們都不善於表達自己的情感，但你們絕對是我堅持下去的唯一動力，今後我也將繼續努力，為我們更美好的生活不斷地前進。

Contents

摘要……..……...i

Abstract……..……...ii

Acknowledgement……iii

Contents……..……..iv

List of Figures……..……...……..……vi

Chapter 1 Introduction

1-1 Introduction to Photonic Crystal Lasers……..1

1-1.1 Photonic Crystals……...1

1-1.2 Photonic Crystal Band Structure……...3

1-1.3 Photonic Crystal Lasers……8

1-2 Introduction to Flexible Devices……...…12

1-2.1 Applications of Flexible Substrate……...……12

1-2.2 Tunable Lasers……13

1-3 Motivation and Overview of Thesis……...……14

Chapter 2 Fabrication and Measurement

2-1 Introduction to Fabricating Instruments……15

2-1.1 Scanning Electron Microscope……15

2-1.2 Plasma-Enhanced Chemical Vapor Deposition……...16

2-1.3 Electron-Beam Lithography……17

2-1.4 ICP/RIE Dry Etching……...18

2-1.5 Wafer Bonding to PDMS Substrate……20

2-2 Fabrication Process of Photonic Crystal Lasers……22

2-3 Micro-PL Measurement Setup……26

2-4 Conclusions……27

Chapter 3 Lasing Characteristics of Photonic Crystal Square Lattice Nanorods

3-1 Lasing Performance on Flat PDMS Substrate……28

3.1-1 Measurement Result……29

3.1-2 Photonic Crystal Band-Edge Mode……32

3-2 Lasing Characterization with Different r/a Ratio……34

3-3 Conclusions……36

Chapter 4 Lasing Characteristics on Flexible Platform

4-1 Calibration of Lattice Extension Percentage……..37

4-2 Lasing Characteristics of Photonic Crystal Lattice Extended along Γ-X Direction...41

4-2.1 Experimental Results……41

4-2.2 Simulation Results……..44

4-3 Lasing Characteristics of Photonic Crystal Lattice Extended along Γ-M Direction..47

4-3.1 Experimental Results……47

4-3.2 Simulation Results……..50

4-4 Conclusions……53

Chapter 5 Summary and Future Works

Reference

List of figures

Figure 1-1.1 Photonic crystals in nature (a) Opal (b) Phosphor powder of the butterfly……...2

Figure 1-1.2 Examples for one-, two-, and three-dimensional photonic crystals. The different colors represent materials with different dielectric constants…….2

Figure 1-1.3 Illustration of a one-dimensional photonic crystal structure…….4

Figure 1-1.4 (a) Lattice of a 1-D photonic crystal structure (b) The corresponding first Brillouin zone and irreducible Brillouin zone…….4

Figure 1-1.5 Photonic band structure with index of (a) 13 and 10 (b) 13 and 7 (c) 13 and 4 (d) 13 and 1. Colored regions indicate the first photonic band gaps……5

Figure 1-1.6 A reflectivity spectrum of a DBR structure in 1-D photonic crystals……5

Figure 1-1.7 Illustration of 2-D photonic crystal square-lattice rods structure……..6

Figure 1-1.8 Illustration of 2-D photonic crystal triangular lattice holes structure……6

Figure 1-1.9 (a) Illustration of the 2-D photonic crystal rods in square-lattice (b) The corresponding first Brillouin zone (c) The irreducible Brillouin zone……...6

Figure 1-1.10 Photonic band structure for both TE and TM modes of square-lattice photonic crystal rods structure……...7

Figure 1-1.11 Configuration of the first demonstrated photonic crystal laser with two-dimensional structure……..8

Figure 1-1.12 (a) The top-view SEM image of the defect region. (b) The simulated mode profile of the lasing node. (c) Spectrum for the laser both above threshold and below threshold. (d) L-L curve for the defect laser……9

Figure 1-1.13 varied geometries of photonic crystal defect cavity ……...9

Figure 1-1.14 The schematic structure of a photonic crystal band-edge laser with triangular hole lattice…….10

Figure 1-1.15 (a) Lasing mode at Γ point of the band structure. (b) L-L curve for the band-edge laser. (c) Lasing spectrum of the Γ-point mode……...11

Figure 1-1.16 (a) Illustration of the square lattice rods structure (b) Cross section view (c) Band-edge mode at Γ point above light line on the band structure (d) L-L curve (e) Lasing spectrum of the band-edge laser in rods square lattice……..11

Figure 1-2.1 Examples for flexible displays consist of OLED……...……12

Figure 1-2.2 Illustration of devices on flexible PDMS substrate. (a) Semiconductor microdisk (b) Triangular-lattice photonic crystal band-edge structure……..12

Figure 1-2.3 Schematic diagram of the wavelength tunable laser. To apply mechanical stress on the flexible substrate make wavelength altered……...13

Figure 2-1.1 The scanning electron microscope system……..15

Figure 2-1.2 Picture of the plasma-enhanced chemical vapor deposition system……...16

Figure 2-1.3 Cross section view of air holes pattern defined on PMMA…….18

Figure 2-1.4 Picture of ICP/RIE system……...19

Figure 2-1.5 Cross section view for SiNx etching (a) grating (b) air hole……...20

Figure 2-1.6 Cross section view for InP etching (a) grating (b) air hole…….20

Figure 2-1.7 Sylgard® 184 A and B from Dow Corning®……..21

Figure 2-2.1 Illustration of the flexible photonic crystal square-lattice rods laser device structure…….22

Figure 2-2.2 The epitaxial structure of InGaAsP QWs……23

Figure 2-2.3 The PL spectrum of the InGaAsP/InP MQWs…….23

Figure 2-2.4 The picture of the fabricated structure on a PDMS substrate……..24

Figure 2-3.1 Picture of micro-PL measurement system……...26

Figure 3-1.1 The SEM image of a field size consists of 5×5 array with different lattice constant…….28

Figure 3-1.2 (a) Pumping spot is converged to focus on the center of the photonic crystal square-lattice rods structure on flexible PDMS substrate. (b) The zoom-in SEM image of photonic crystal square-lattice rods structure with 705 nm lattice constant and 0.37 r/a ratio……...29

Figure 3-1.3 PL spectrum of MQWs on flexible PDMS substrate……..29

Figure 3-1.4 Lasing spectrum from photonic crystal square-lattice rods structure with 705 nm lattice constant……...……30

Figure 3-1.5 Light in & Light out curve (L-L curve) and Linewidth of the lasing peak…….30

Figure 3-1.6 Lasing wavelength increases as the lattice constant increases. The normalized frequency is estimated around 0.44……...……31

Figure 3-1.7 2-D PWE simulated TE-like band structure of the photonic crystal square-lattice structure…….32

Figure 3-1.8 Optical mode profile calculated for H_z field of TE mode by 3-D FEM simulation……..33

Figure 3-2.1 Lasing spectrum from devices of different r/a ratio in the same lattice constant of 705 nm……...34

Figure 3-2.2 Lasing wavelength and corresponding normalized frequency of devices A to E with different r/a ratio……...34

Figure 3-2.3 Variation of pumped effective power density and quality factor with different r/a ratio in 705 nm lattice constant…….35

Figure 3-2.4 Simulation result for wavelength variation in different r/a ratio and lattice constant of 705 nm. Experimental result is also marked……..36

Figure 4-1.1 Image of the homemade stage which serves as the extending platform. Sample is fixed on the stage by two clamps and extended by rotating the micrometer……....38

Figure 4-1.2 Zoom-in picture of sample on the homemade extending stage. The distance between two red lines is 5 mm……..38

Figure 4-1.3 SEM picture of calibrated sample. Marked areas were measured and the corresponding extension percentages were calculated by variation of length to original length…….39

Figure 4-1.4 Lattice extension percentage versus ΔR and ΔX/X. ΔR is rotated distance of micrometer, and ΔX /X is the corresponding sample extension percentage…….40

Figure 4-2.1 Illustration of lattice extended along Γ-X direction……41

Figure 4-2.2 Light-in & light-out curve of the 705 nm flexible photonic crystal square-lattice rods laser with different lattice extension percentage along Γ-X direction……..42

Figure 4-2.3 Lasing spectrum of the 705 nm lattice constant flexible photonic crystal square-lattice rods laser with different lattice extension percentage along Γ-X direction……42

Figure 4-2.4 Lasing wavelength versus the lattice extension percentage along Γ-X direction of the 705 nm lattice constant flexible photonic crystal square-lattice rods laser……43

Figure 4-2.5 Effective threshold power and quality factor of the 705 nm lattice constant flexible photonic crystal square-lattice rods laser with different lattice extension percentage along Γ-X direction……...43

Figure 4-2.6 Illustration of our model for the lattice variation along Γ-X direction……44

Figure 4-2.7 Illustration of a unit cell deviation of photonic crystal square-lattice rods structure with 20 % extended lattice along Γ-X direction……44

Figure 4-2.8 Mode profiles for TE mode in Hz field of photonic crystal square-lattice rods laser with 705 nm lattice constant in different lattice extension percentage along Γ-X direction. (a) Original un-extended square lattice (b) Lattice extension percentage of 4 % (c) Lattice extension percentage of 10 %.....45

Figure 4-2.9 Comparison between experimental result and simulated result with extended lattice along Γ-X direction……46

Figure 4-2.10 Comparison of wavelength tunability slop between experiment and simulation with varied r/a ratio……...46

Figure 4-3.1 Illustration of lattice extended along Γ-M direction……47

Figure 4-3.2 Light-in & light-out curve of the 705 nm photonic crystal square-lattice rods laser with different lattice extension percentage along Γ-M direction……..48

Figure 4-3.3 Lasing spectrum of the 705 nm photonic crystal square-lattice rods laser with different lattice extension percentage along Γ-M direction……..48

Figure 4-3.4 Lasing wavelength versus the lattice extension percentage along Γ-M direction of the 705 nm lattice constant photonic crystal square-lattice rods laser……..49

Figure 4-3.5 Effective threshold power and quality factor of the 705 nm lattice constant photonic crystal square-lattice rods laser with different lattice extension percentage along Γ-M direction……49

Figure 4-3.6 Illustration of our model for the lattice variation along Γ-M direction……...50

Figure 4-3.7 Illustration of a unit cell deviation of photonic crystal square-lattice rods structure with 20 % lattice extension along Γ-M direction……...50

Figure 4-3.8 Mode profiles for TE mode in Hz field of photonic crystal square-lattice rods laser with 705 nm lattice constant in different lattice extension percentage along Γ-M direction. (a) Original un-extended square lattice (b) Lattice extension percentage of 4 % (c) Lattice extension percentage of 10 %.....51

Figure 4-3.9 Comparison between experimental result and simulated result with extended lattice along Γ-M direction……52

Figure 4-4.1 Comparison of wavelength tunability between lattice extension along Γ-X and Γ-M direction……53

Chapter 1

Introduction

1-1 Introduction to Photonic Crystal Laser

In the world, the first laser had been demonstrated by Theodore H. Maiman in 1960. Later in 1962, Robert N. Hall demonstrated the first semiconductor laser diode device, made of gallium arsenide (GaAs) and emitted at 850 nm the near-infrared band of the spectrum. Since then, much interest was attracted to scientists in developing a wide variety of lasers including semiconductor laser, solid state laser, and gas laser, etc. In the present, laser products are widely applied in the world and take an important role in our life. For example, CD player, laser pointer, and industrial cutting laser have been necessaries in our life for a long time.

These days the technique in optical communication becomes more and more important, so a compact and efficient laser light source at long wavelength is very necessary for optical communication networks. Vertical-cavity surface-emitting laser (VCSEL) is commonly applied in 1.55 um optical communication wavelength but it still has some disadvantages like fabrication difficulties, a larger mode volume, higher threshold power, and lower quality factor. However, with some physics effects in photonic crystal structure, the photonic crystal laser could be applied to and it can conquer those obstacles mentioned above.

1-1.1 Photonic Crystals

Photonic crystals are one type of nanostructures which composed of periodic dielectric materials. In general, photonic crystals contain regularly repeating internal regions of high and low dielectric constant, which affecting the propagation of electromagnetic waves in the same way as the periodic potential in a semiconductor crystal affects the electron motion by defining allowed and forbidden electronic energy bands. In fact, photonic crystal occurs in nature and in various forms that have been studied scientifically for the last 100 years. Lord Rayleigh started their study in 1887, by showing that such systems have a spectral range of large reflectivity, which was known as a stop-band [1]. We call the stop-band ‘photonic band gap’ in optical field these days. Figure 1-1.1 shows such examples for photonic crystals structure in nature.

(a) (b)

Figure 1-1.1 Photonic crystals in nature (a) Opal (b) Phosphor powder of the butterfly

*http://www.gemstones-guide.com/Opal

*http://www.nhm.ac.uk/about-us/news/2008/july/how-wings-shimmer-revealed18265/

Although photonic crystals have been studied in one form or another for a long time, the concept “photonic crystal” was first discussed over 100 years later, after Eli Yablonovitch [2] and Sajeev John [3] published two milestone papers on photonic crystals in 1987. They found out that periodic structures with different dielectric constants could effectively control the behaviors of light. These new concepts attracted attentions from the world and “photonic crystal” was named later in the year.

Photonic crystals structure could be separated to three different types; those are one-dimensional (1-D), two-dimensional (2-D) and three-dimensional (3-D) photonic crystals. Figure 1-1.2 shows the illustrations of 1-D, 2-D and 3-D photonic crystals structure from left to right. The 1-D and 2-D photonic crystals have been widely used in applications of practical devices in recent years. However, the 3-D photonic crystals are still in the phase of research and development because of its difficulties in fabrication.

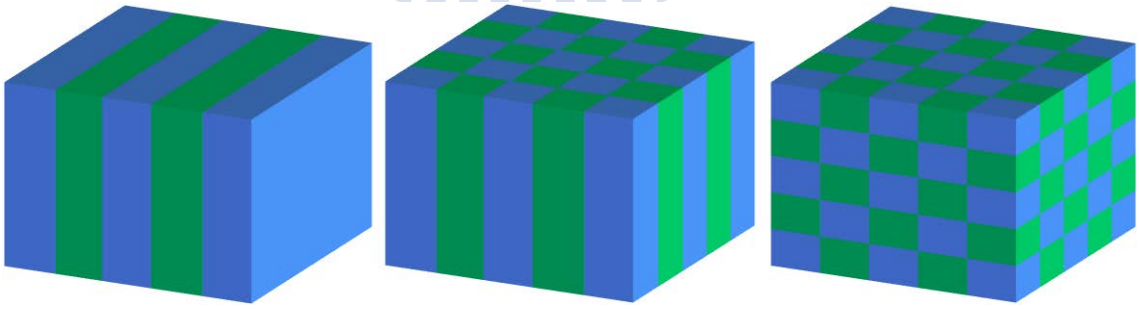

1-D 2-D 3-D

Figure 1-1.2 Examples for one-, two-, and three-dimensional photonic crystals. The different colors represent materials with different dielectric constants.

1-1.2 Photonic Crystal Band Structure

In order to understand the especial photonic band gap and photonic band structure, it will be easier to investigate from the concept of a mature theorem of electronic band. In the conventional electronic band structure theorem, the periodic lattice structure could affect the motion of electrons, which is defined by the Schrödinger equation,

$$[-\frac{\hbar^2}{2m} + \mathrm{V(r)}]\Psi(\mathrm{r}) = \mathrm{E}\Psi(\mathrm{r}) \tag{1.1}$$

In the equation, V(r) stands for the potential function induced by periodic lattice structure, and Ψ(r) represents the possibility of electrons that exist in space. When we solve the equation, Ψ(r) becomes zero in some specific energy level. That is to say, there is no any electron in the energy level, which is the well-known term electron band gap.

The photonic crystals have the similar periodic structure like periodic lattice structure in solid state physics. The periodic variation constructed by materials with high index and low index supports a similar potential function such in lattice structure to affect the behaviors of photons in photonic crystal, which is described with the following equation,

$$\nabla \times (\frac{1}{\varepsilon(r)} \nabla \times \mathrm{H(r)}) = (\frac{w}{c})^2 H(r) \tag{1.2}$$

In the equation, ε(r) defines the function of index variation in space. With the given ε(r), we could solve the corresponding H(r) magnetic distribution in varied frequency. In this way we can find out the eigenvalue and eigenvector step by step. Therefore the photonic crystal band diagram could be solved. The solution of H(r) is an exponential decayed term in some specific frequency division, indicating those specific frequencies propagate in the given photonic crystals structure and decay in the end. That is to say, light with the specific frequency is forbidden in the photonic crystals; thus the forbidden band is formed.

One-dimensional Photonic Crystal

One-dimensional photonic crystals consist of thin dielectric layers with periodic index variation. Figure 1-1.3 shows the illustration of one-dimensional photonic crystal structure. Figure 1-1.4(a) shows the lattice illustration of 1-D photonic crystal structure with lattice constant of a, and (b) is the corresponding Brillouin zone. The first Brillouin zone is in the interval between -π/a to +π/a, and the irreducible Brillouin zone is form by the interval 0 to +π/a.

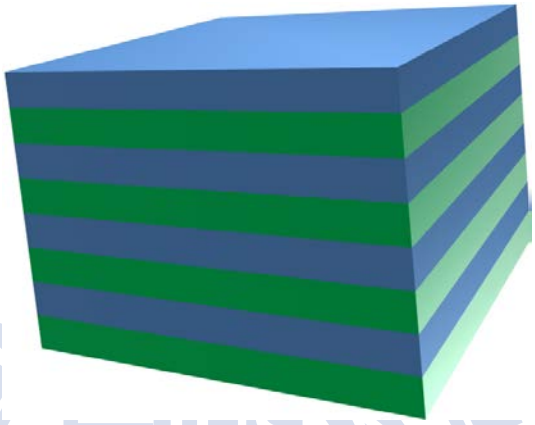

Figure 1-1.3 Illustration of a one-dimensional photonic crystal structure

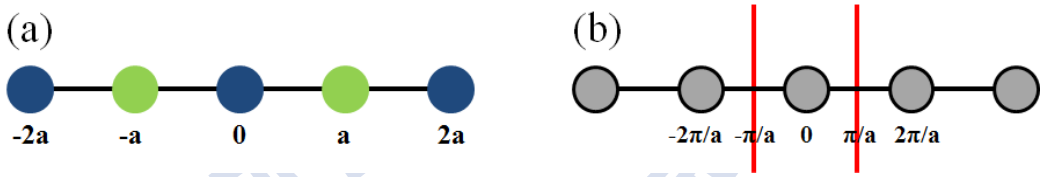

Figure 1-1.4 (a) Lattice of a 1-D photonic crystal structure (b) The corresponding first Brillouin zone and irreducible Brillouin zone.

We can roughly calculate the photonic band structure with simple codes of plane-wave-expansion (PWE) method by MATLAB software. The calculated 1-D photonic crystal structure consists of periodic layers with equal thickness that have high index of 13 dielectric constant and low index varied from 10 to 1 dielectric constant. Figure 1-1.5 (a) to (d) show the calculated band structures, the colored regions indicate the first band gaps between first band and second band. From these charts we could observe that band gap size becomes larger as the varied low index decreases. It implies that the larger index difference of the 1-D photonic crystal, the larger gap size is. In the band structure, the y-axis indicates the normalized frequency, which is divided by lattice constant to lambda. By tuning the lattice constant or index difference of the structures, we can choose a proper region with specific modes for applications.

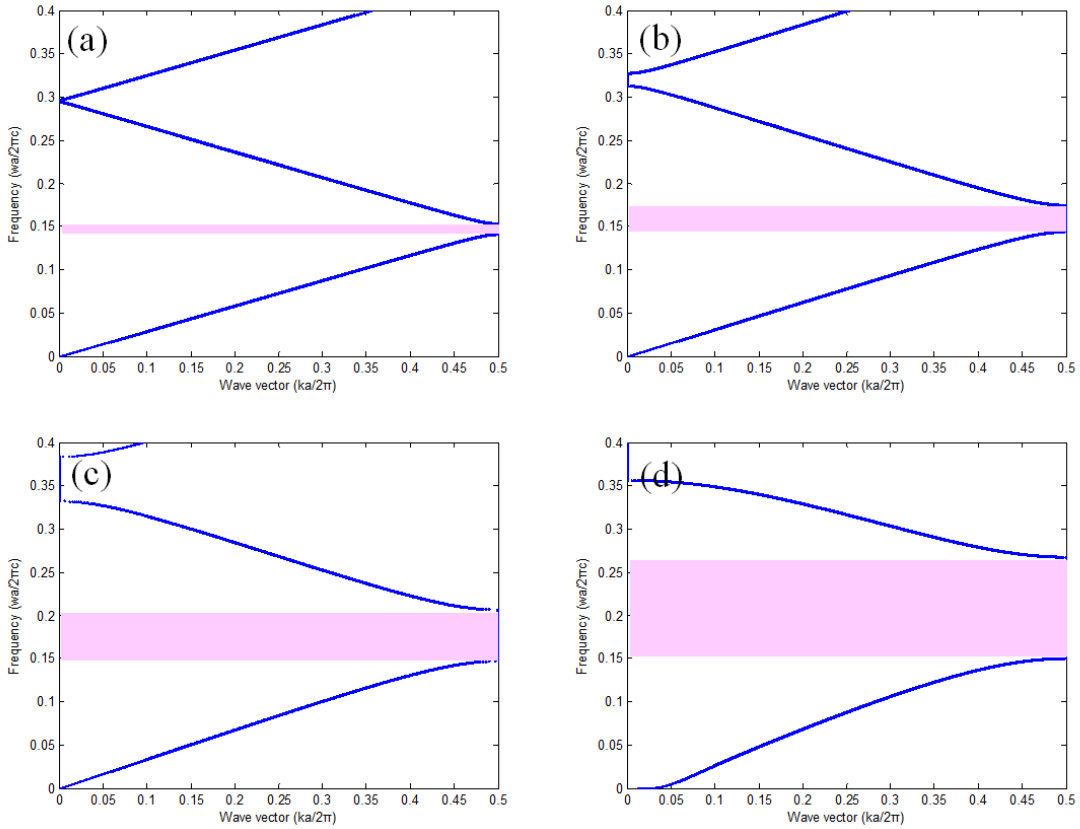

Figure 1-1.5 Photonic band structure with index of (a) 13 and 10 (b) 13 and 7 (c) 13 and 4 (d) 13 and 1. Colored regions indicate the first photonic band gaps.

Figure 1-1.6 shows an example for application of 1-D photonic crystals [4]. The structure consists of 12 repeat silicon oxide/silicon nitride λ/4 pairs which is called distributed Bragg reflector (DBR) structure. The reflectivity of the wavelength in 480~600 nm approaches 100 % because the photonic band gap of the structure is in this region. It indicates the light with frequencies in the band gap will be reflected and others penetrate through the DBR structure. Much application with these 1-D photonic crystals is introduced to solar cells.

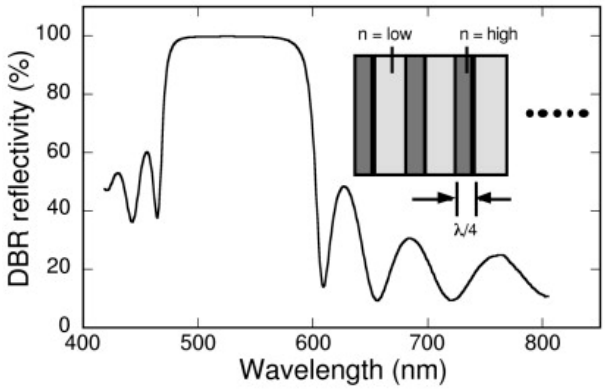

Figure 1-1.6 A reflectivity spectrum of a DBR structure in 1-D photonic crystals [4]

Two-dimensional Photonic Crystal

Two-dimensional photonic crystals are commonly constructed by 2D periodic arrays with triangular-lattice or square-lattice. Figure 1-1.7 illustrates the 2-D photonic crystal rods structure in square-lattice with high dielectric constant. Figure 1-1.8 illustrates the 2-D photonic crystal air holes structure in triangular-lattice drilled in a membrane.

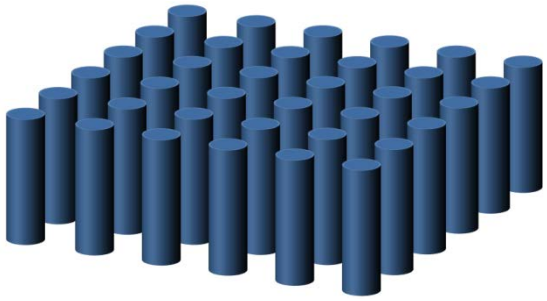

Figure 1-1.7 Illustration of 2-D photonic crystal square-lattice rods structure

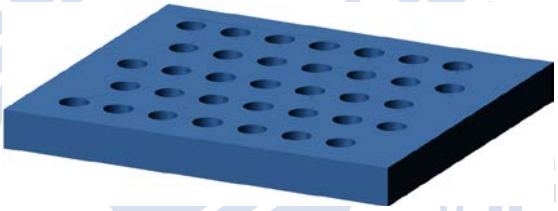

Figure 1-1.8 Illustration of 2-D photonic crystal triangular lattice holes structure

We take the square-lattice rods structure as the example for 2-D photonic crystals. Figure 1-1.9 shows the illustration of square-lattice rods in real space. The first Brillouin zone and irreducible Brillouin zone in reciprocal space are also shown in Figure 1-1.9(b) and (c), respectively. There are three symmetry point denoted ‘Γ’, ‘X’ and ‘M’.

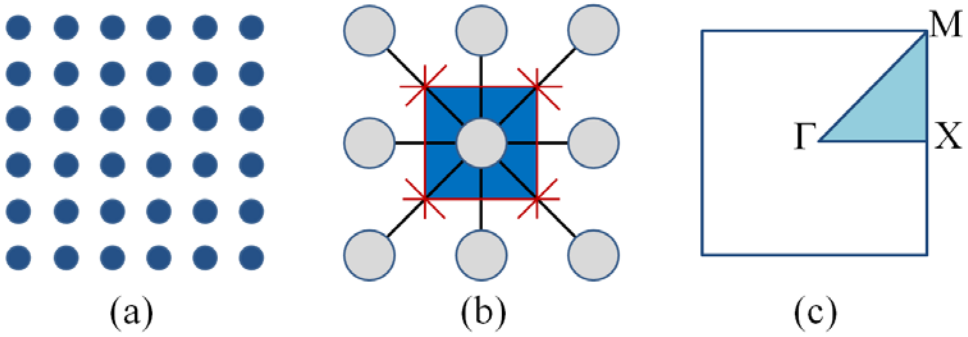

Figure 1-1.9 (a) Illustration of the 2-D photonic crystal rods in square-lattice (b) The corresponding first Brillouin zone (c) The irreducible Brillouin zone

Figure 1-1.10 is the photonic band structure for both TE and TM modes of square-lattice photonic crystal rods structure [5]. The structure consists of alumina rods with r/a ratio of 0.2 embedded in air. In this chart, blue band represent TM modes, and red band represent TE modes. We can find out that there is no band gap in TE modes but large band gap size around 0.15 is observed in TM mode.

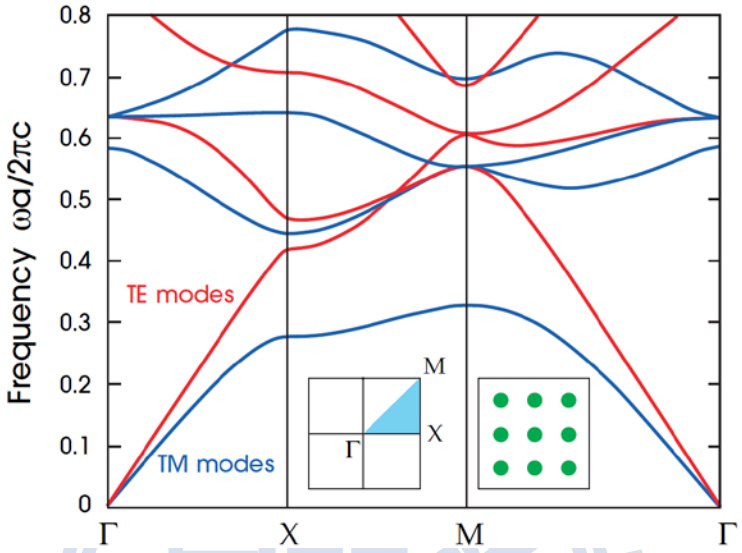

Figure 1-1.10 Photonic band structure for both TE and TM modes of square-lattice photonic crystal rods structure [5]

1-1.3 Photonic Crystal Lasers

One of the important applications of photonic crystals structure is photonic crystal laser. The traditional lasers consist of four basic factors: resonator, gain medium, excitation system, and output coupler. The idea of a laser resonator formed by photonic crystal was first proposed in 1994 [6]. With a well-designed resonant cavity fabricated in high refractive index gain materials for specific wavelength, light could be attracted in the resonant cavity and amplified by interaction with gain mediums; hence the photonic crystal laser structure could achieve lasing when threshold condition is reached under the optical or electrical pumping. In general, photonic crystal lasers are separated into two categories with different resonant cavity types: photonic crystal defect laser and photonic crystal bane-edge laser. The two different type photonic crystal lasers will be introduced individually below.

Photonic Crystal Defect Laser

Photonic crystal band gap is the main role in photonic crystal defect laser. Light with the forbidden frequency of the photonic band structure will be localized and resonate in the defect region. The first photonic crystal laser with defect cavity is demonstrated by the O. Painter group from Caltech in 1999 [7]. Figure 1-1.11 shows the illustration of their photonic crystal laser structure. The air holes were defined by electron-beam lithography and dry plasma etching into the slab. In sequence the InP substrate was removed by wet etching, thus forming an active luminescence layer surrounded by air. Also photons are localized vertically by (Total internal reflection) TIR due to index difference at the air-slab interface. The combination of photonic band gap effect from the 2-D photonic crystal and TIR from the low-index cladding results in a three-dimensionally confined optical mode. Figure 1-1.12 shows the top-view SEM image, mode profile, lasing spectrum, and L-L curve of the defect laser.

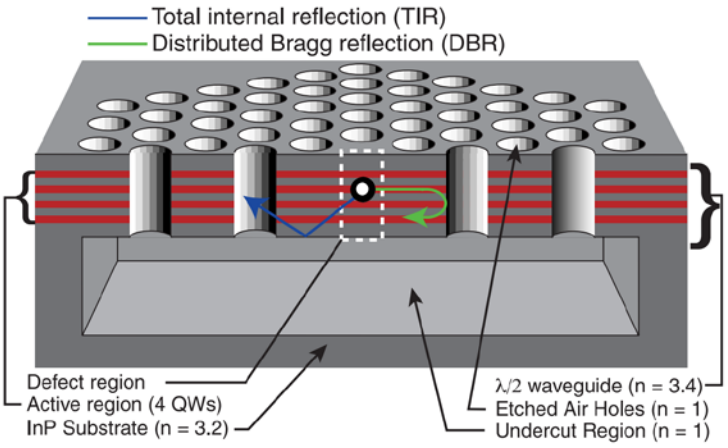

Figure 1-1.11 Configuration of the first demonstrated photonic crystal laser with two-dimensional structure [7]

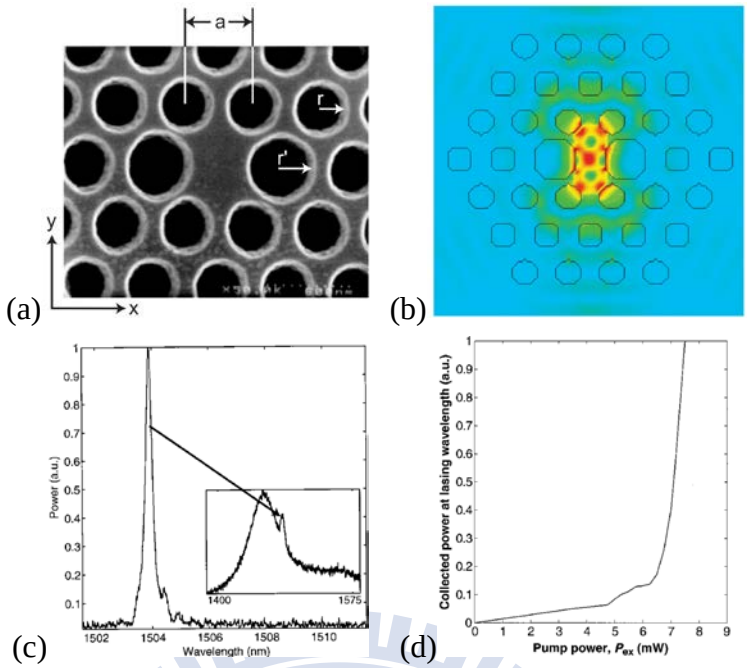

Figure 1-1.12 (a) The top-view SEM image of the defect region. (b) The simulated mode profile of the lasing node. (c) Spectrum for the laser both above threshold and below threshold. (d) L-L curve for the defect laser [7].

After the first photonic crystal laser was demonstrated, some ideas for the geometry of resonant cavities were discussed in order to improve the lasing characterizations of photonic crystal defect lasers. In 2002, the group of O. Painter also fine-tuned the position and dimension of air holes in their photonic crystal defect structure to generate and control different defect modes [8]. As shown in Figure 1-1.13, in this way the characteristics of the dipole modes in a single defect could be altered due to effective refractive index variation in specific direction after fine-tuning the air holes.

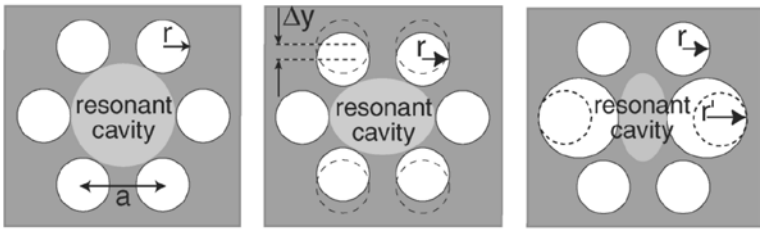

Figure 1-1.13 varied geometries of photonic crystal defect cavity [8]

In recent years, people around the world put lots of works on 2-D photonic crystal defect lasers. Abundant varieties of nanocavity such as point-shift cavity [9], were demonstrated to pursue the potential advantages of small mode volume, abilities to achieve ultra-high quality factor and low threshold power.

Photonic Crystal Band-edge Laser

Dissimilar to photonic crystal defect laser, photonic crystal band-edge laser utilize the concept of slow light [10] with flat band near the band-edge in the photonic band structure. The idea was brought up in 1994. [11] At the band edges such as Γ, X, M points for square lattice structure, standing waves are formed by the superposition of reflected waves originating from the periodic index variation. Therefore, near the symmetry points, the group velocity of wave approaches zero and the density of photon states becomes infinity. Once the group velocity is slowed down, photons would have much longer time to interact with gain medium thus lasing action from the photonic crystal structure could be expected.

The photonic crystal band-edge laser was first demonstrated by the group of S. Noda in 1999 [12]. Figure 1-1.14 shows the configuration of the laser. The triangular-lattice holes membrane was embedded by the wafer fusion technique. The interaction between photonic crystal band-edge mode and gain medium contribute lasing action but the quality factor and threshold current are not good compared to the photonic crystal defect laser because of low index contrast between active layer and outer cladding layer. However, the characteristics of high output power and small divergence angle were observed in this band-edge laser. Figure 1-1.15(a) shows the calculated band structure, the band-edge lasing mode occur on the Γ symmetry point, which is denoted A and B in detailed picture. Also the light-in light-out curve and lasing spectrum of the photonic crystal band-edge laser are shown in Figure 1-1.15 (b) and (c).

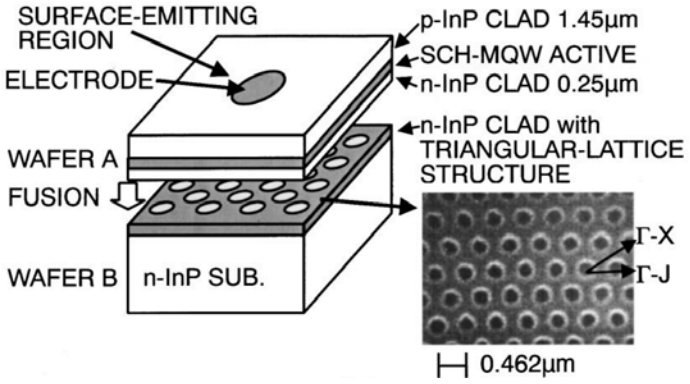

Figure 1-1.14 The schematic structure of a photonic crystal band-edge laser with triangular hole lattice. [12]

Generally speaking, the band-edge lasers suffer larger loss in lateral direction than the defect lasers because band-edge modes are not in photonic band gap. In 2004, a tapered structure similar to hetero-structure was introduced to overcome the problem [13]. The slight variation of refractive index in the tapered structure suppresses the lateral loss, decreasing mode distribution in leaky region and high quality factor could be observed. Some famous

structures like “heterostructure” [14] and “nanobeam” [15] are originated from this concept to pursue ultra-high quality factor, small mode volume and further better lasing performance.

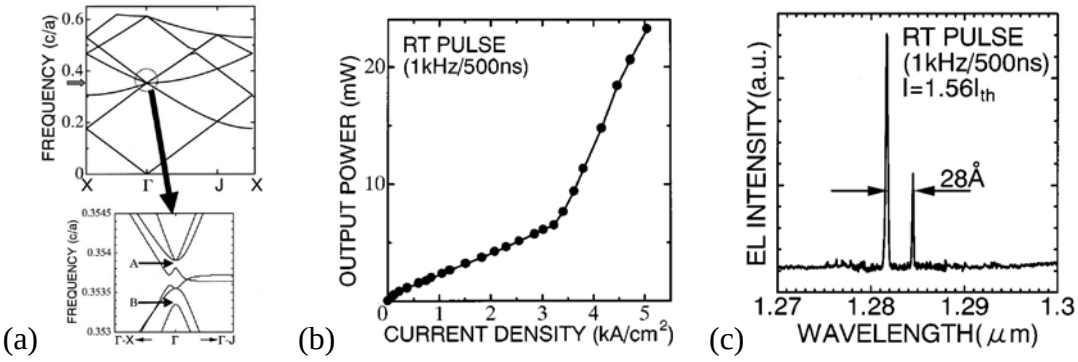

Figure 1-1.15 (a) Lasing mode at Γ point of the band structure. (b) L-L curve for the band-edge laser. (c) Lasing spectrum of the Γ-point mode. [12]

From 1999 the first photonic crystal laser was published, most 2-D photonic crystal is commonly a lattice of holes fabricated in slab. The first band-edge laser with square lattice rods was demonstrated by L. Ferrier et al. after a long time in 2009 [16]. Figure 1-1.15 (a) and (b) shows the illustration of the square lattice structure consists of high index InP rods bended to low index silica Bragg Mirror. They demonstrated that the use of rods in place of holes could make carries confined in rods and cannot diffuse outside the pumping area. In this way an accurate control of carrier injection can be achieved even if the lateral confinement is not good enough. In addition the lasing mode at Γ symmetry point above light line indicates a surface emitting laser, which is the most proper laser light source for applications on the integrated photonic circuit []. Figure 1-1.15 (c) is the lasing mode on band structure; L-L curve and lasing spectrum are also shown in (d) and (e).

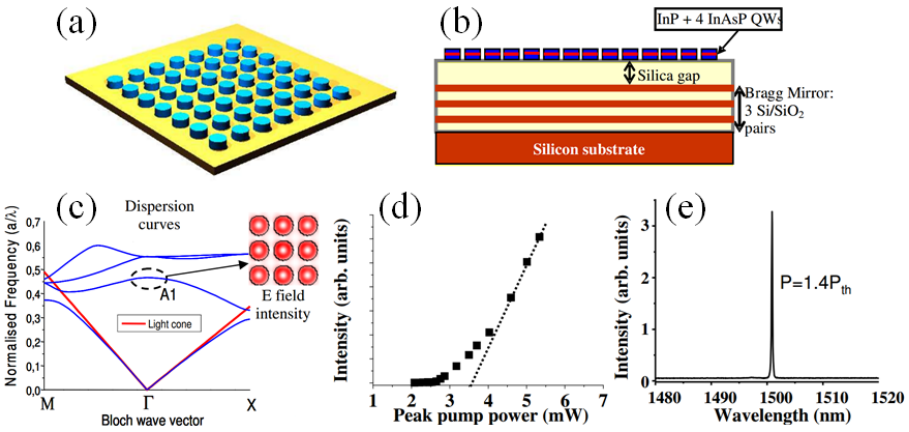

Figure 1-1.16 (a) Illustration of the square lattice rods structure (b) Cross section view (C) Band-edge mode at Γ point above light line on the band structure (d) L-L curve (e) Lasing spectrum of the band-edge laser in rods square lattice [16]

1-2 Introduction to Flexible Devices

1-2.1 Applications of Flexible Substrate

The polymer/organic photonic devices had been widely studied because of their special spectral properties and application flexibility. Many applications in a flexible platform had been demonstrated such as light source [17], modulators [18], sensors [19] and displays [20] and so on. Compared to other inorganic optical devices, polymer has many unique features including its good elastic property. Polymers can be elongated by over 10 % before they reach their elastic limits, whereas less than 1 % of elongation is available in common semiconductor hard substrate. Figure 1-2.1 shows the OLED displays on flexible platform.

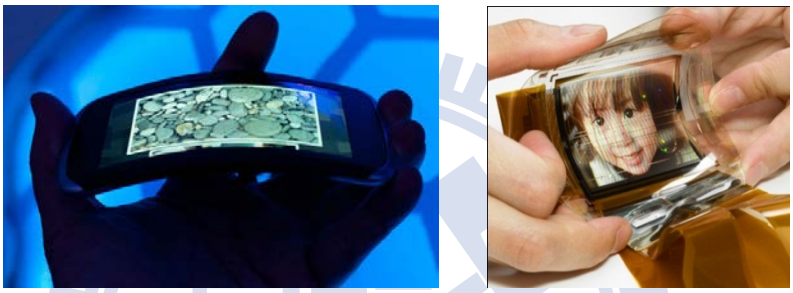

Figure 1-2.1 Examples for flexible displays consist of OLED.

*http://www.techrollin.com/mobile-app/nokia-unveils-kinetic-flexible-oled-display/

*http://tech4teacher.wordpress.com/tag/flexible-display/

In our previous works, we have demonstrated various optical devices fabricated on the flexible PDMS substrate Figure 1-1.2(a) shows a semiconductor microdisk device which is suited to be a compact light source with low threshold power or curvature sensor in photonic integrated system [21-23]. The triangular-lattice photonic crystal band-edge laser as illustrated in Figure 1-2.2(b) could be a local curvature sensor or a multi-wavelength light source used in integrated photonic circuit with a very compact size [24].

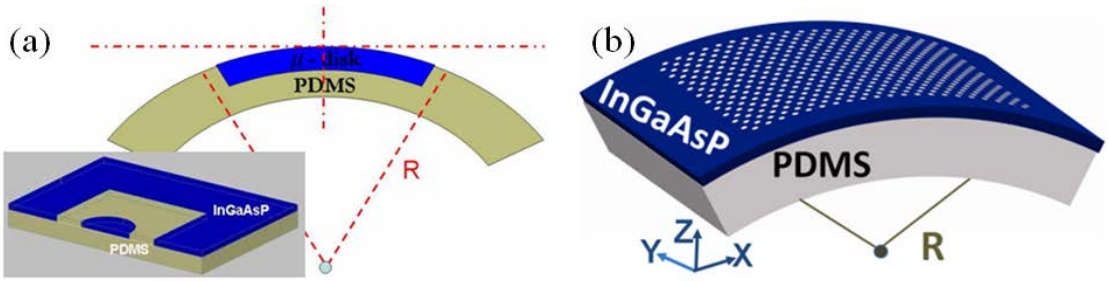

Figure 1-2.2 Illustration of devices on flexible PDMS substrate. (a) Semiconductor microdisk [21-23] (b) Triangular-lattice photonic crystal band-edge structure [24]

1-2.2 Tunable Lasers

Wavelength tunable lasers have attracted attentions since 30 years ago [25]. Much investigation was improved to extend the wavelength tuning range for covering the entire bandwidth for wavelength division in optical communications [26]. The term 'tunable laser' refers to a single-mode laser on flexible substrate, for which the lasing wavelength can be adjusted through an external stimulus. Compared to single fixed wavelength semiconductor lasers, tunable lasers reduce the complexity of fabricating a series of lasers with various specific wavelengths corresponding to the Wavelength Division Multiplexing (WDM) grids; hence economizing the cost on fabrication. These devices are available for a wide tuning range of wavelengths and for several application fields such as telecommunications and biomedical sensing.

Figure 1-2.3 shows an example for a tunable laser based on the strain tuning of a flexible polymer substrate [27]. The device consists of Bragg grating on the flexible substrate could be imposed by both tensile and compressive strains; hence inducing a larger tuning range.

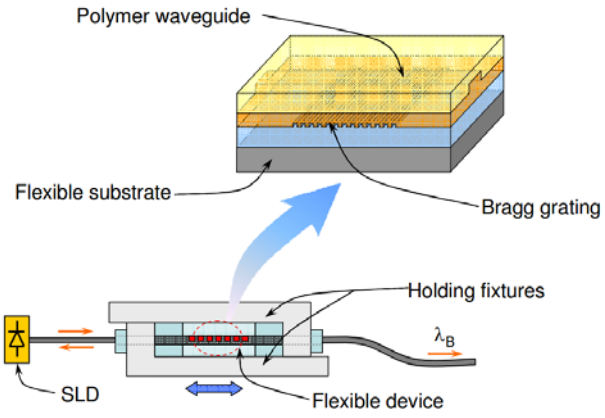

Figure 1-2.3 Schematic diagram of the wavelength tunable laser. To apply mechanical stress on the flexible substrate make wavelength altered. [27]

1-3 Motivation and Overview of Thesis

The long wavelength photonic crystal lasers, which have been widely studied and discussed, is a potential light source for the optical communication networks in the future. There are several attractive features in these lasers including low threshold power, high output power, a high density compact size device, and high enough quality factor that retain the integrity of signals in the process of optical communication. In addition, photonic crystal lasers could be fine-tuned in the geometry to serve as the high-resolution tunable laser light source for the Wavelength Division Multiplexing (WDM) system in photonic integrated circuits.

However, the wavelength of general photonic crystal defect lasers or band-edge lasers are fixed to specific values once the devices are fabricated on a hard semiconductor substrate. If we construct a group of photonic crystal lasers with various lasing wavelength, the cost will increase highly and the compactness in high dense photonic integrated circuits becomes impractical. Fortunately, a widely used and low-cost polydimethylsiloxane (PDMS) material could serve as a flexible substrate for fine-tuning the geometry of the photonic crystal laser structure. We want to combine the features of compactness in photonic crystals and flexibility in flexible materials to realize a semiconductor device which has larger application flexibility with a compact size.

In this thesis, we demonstrate the multi-wavelength square-lattice photonic crystal band-edge rods laser with a flexible PDMS substrate. The optical properties of the lasing mode can be altered by extending the lattice constant with a homemade extending stage. Both the lattice extension along Γ-X and Γ-M direction are demonstrated. Moreover, we perform 2-D plane-wave-expansion (PWE) method and 3-D finite-element method (FEM) to characterize the lasing mode and variation in wavelength for the same phenomenon of this tunable laser. Comparing the simulation to the experimental result, we can further understand the lasing characterization and deduce the behaviors in wavelength variation of the laser with different lattice extension percentage.

With the flexible technology applied in photonic crystal lasers, we can easily fine-tune the lasing wavelength. As a result we can only fabricate a single device to achieve a reliable multi-wavelength photonic crystal tunable laser rather than fabricate lots of devices for specific wavelengths with different geometry in a large dimension. In this way, the cost for the multi-wavelength devices could be reduced and application flexibility in high dense compact photonic integrated circuits becomes much practicable.

Chapter 2

Fabrication Procedures and Measurement Setups

In this chapter, I will briefly introduce the fabrication instruments which are used in fabricating the photonic crystal rods laser devices and how to make the feasible PDMS substrate. Then I will show the detailed fabrication steps for flexible photonic crystal rods laser.

2-1 Introduction to the Fabrication Instruments

2-1.1 Scanning Electron Microscope (SEM) System

The scanning electron microscope system really takes an important role for micro-scale photonic devices fabrication. In order to assure whether the devices are successfully fabricated, it helps us check the geometry parameters in each fabrication process. Besides, we can perform simulations with those parameters to further understand the lasing data we recorded. The SEM system acts as the eye in fabrication process flow. Figure 2-1.1 shows the scanning electron microscope system. The system model is Inspect F from FEI Company.

Figure 2-1.1 The scanning electron microscope system.

2-1.2 Plasma Enhanced Chemical Vapor Deposition (PECVD) System

We have to deposit silicon nitride (SiN_x) layer as a hard mask layer on the epitaxial wafer for the following fabrication process. We use the Oxford plasmalab 80 plus to deposit 240 nm thickness SiN_x on the epitaxial wafer with $SiH_4/NH_3/N_2$ mixture gases. The SiN_x thin film quality strongly depends on the NH_3/ SiH4 gas ratio. The SiN_x thin film deposited with NH_3 addition would be easy for chemical etching process. Actually, the SiN_x layer can also be deposited at absence of NH_3 gas. In this way, the resistance to InP dry etching will be much higher, but the SiN_x layer cannot be removed completely by the BOE wet etching. It is a trade off because the high resistance to dry etching is good for the InP etching but it is hard for the pattern on PMMA to be transferred to SiN_x layer. As a result, we tried different recipes by changing NH_3/ SiH_4 ratio and find the acceptable recipe for the fabrication procedures. Finally, the equal amount of NH_3 and SiH_4 gases is used for the SiN_x deposition. We deposit SiN_x layer with 8 sccm SiH_4, 8 sccm NH_3, 250 sccm N_2. The RF power is 20 w, the temperature is 200°C, and the chamber pressure is 1000 mtorr .

Figure 2-1.2 Picture of the plasma-enhanced chemical vapor deposition system

2-1.3 E-beam Lithography Process

E-beam lithography is used in our sub-micron device fabrication, it is because E-beam lithography has the higher spatial resolution than the traditional photo lithography. We use Polymethylmethacrylate(PMMA) as the high resolution positive resist. PMMA is a polymeric material which has been commonly used in semiconductor industry. It is formulated with 950,000 molecular weight resins in either chlorobenzene or the safer solvent anisole. The ratio of PMMA to anisole is 5/100, which is called A5, and it affects the thickness of coating layer. The more the PMMA dissolve into anisole the thicker the coating layer is for the same spin speed of coating.

After cleaning the SiN_x-deposited wafer surface by Acetone, we spin coat a PMMA layer on the top of the wafer by a spin coater with two steps. The first step, the rotation speed is 1000 revolution per minute (rpm) for ten seconds. It will help the PMMA layer be uniform on the top of the wafer. For the second step, the rotation speed is increased instantly to 3500 rpm for 120 seconds. The PMMA layer becomes much thinner at this step. After coating the PMMA, the wafer is soft baked on hot plate by 180℃ for 120 seconds. It can not only make most of the solvent vaporized but also increase the adhesive ability between PMMA and wafer surface. The PMMA would be harder after baking, and the thickness would be around 300 nm after these steps.

As mentioned above, we use the e-beam lithography process to define the patterns on the PMMA layer which was spin coated on the SiN_x-deposited wafer. The patterns that stored in computer are direct written on PMMA layer by scanning electron beam with 30kV energy. Electron beam will alter the solubility of the PMMA in exposed area. After e-beam exposure, the exposed area would be developed for 70 seconds by a developer which consists of Isopropanol (IPA) and MIBK with 3:1 ratio. It's worth mentioning that the ratio of IPA and MIBK affects the resolution and sensitivity. The higher percentage of IPA in developer, the higher resolution is; but the sensitivity gets lower. Following we terminate the develop process by pure IPA. The developer is also removed. Finally, we immerse the sample deionized water and dry it by nitrogen gas.

With the Optical Microscope (OM) system, we can check whether the patterns are successfully developed. Figure 2-1.3 shows a SEM image of the cross section view to the air hole patterns after the develop process. The vertical profile of the hole shape and the unmasked SiN_x surface in the bottom of holes indicate that the dosage of e-beam process is appropriate for the pattern and the develop process is successful.

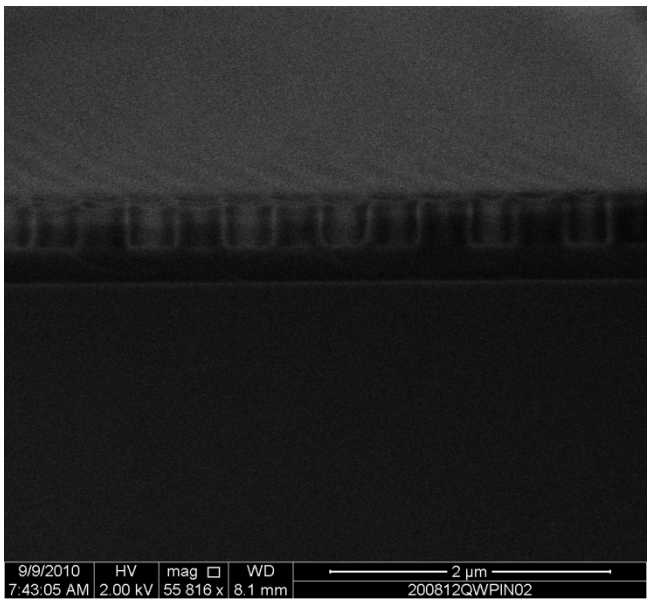

Figure 2-1.3 Cross section view of air holes pattern defined on PMMA

2-1.4 ICP/RIE system

In the fabrication procedures, the patterns on PMMA are transferred to the SiNx and further to InGaAsP layer by dry etching process. The anisotropic etching of dry etching is very common in the semiconductor industry. The key process of the dry etching is the plasma formation. The plasma is a state of matter similar as gases in which part of the particles are ionized. With the well selection of gas types, the active plasma would react with the exposed area and forms the gas-type products which would be pumped out of the system. This kind of reaction is chemical etching process. Sometimes we need some high weight ions to bombard the reactant surface in order to increase the etching rate. Combination of sputtering and chemical etching processes significantly increases etching rate in a specific direction. It may be caused by the higher local temperature of the bombardment area to increase the chemical etching rate. This kind of the etching is called reactive ion etch (RIE) process. If we want to increase the plasma density, we can make the electrons accelerated in angular direction. The RF power is inductivity couples to plasmas, which is called inductive couple plasma (ICP). In this way, we can achieve high plasma density at low temperature. Besides, it allows independent control of ion flux and ion energy, which is feasible for us to control the etching condition.

Our dry etching system is ICP/RIE system, which is shown in Figure2-1.4. The brand model is Oxford Plasmalab system 100. CHF3, O2, N2 and Cl2 are provided for dry etching. We can tune recipes by varying the gas flow, chamber pressure, temperature, RF power and ICP power. The high density plasmas of this system are very useful for fabricating the sub-micron structures with controllable selectivity, sooth morphology, vertical profile and high etching rate.

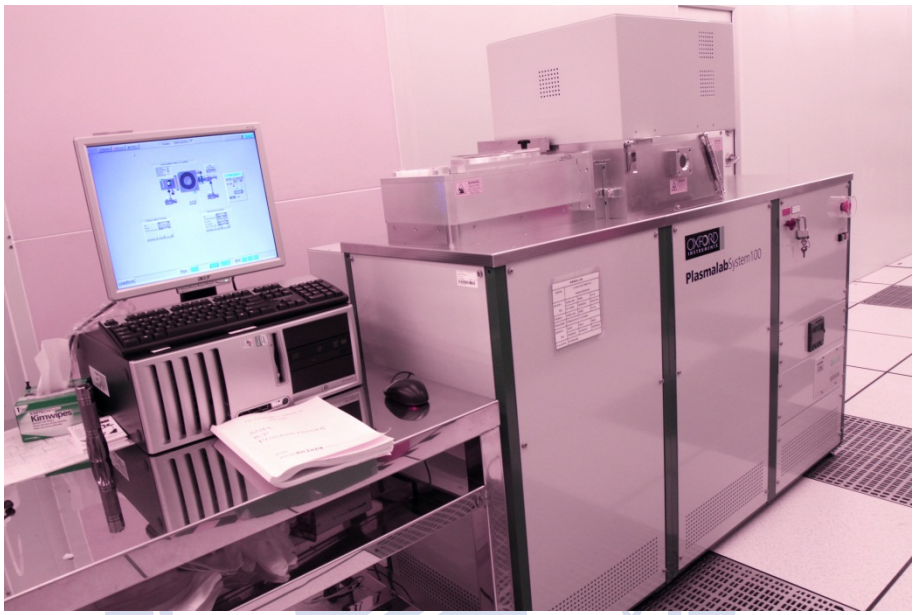

Figure 2-1.4 Picture of ICP/RIE system

The defined patterns are transferred to SiN_x layer by RIE at 20℃with CHF_3：50 (sccm), O_2：5 (sccm), RF power：150 (W) and pressure：55 (mtorr). Figure 2-1.5 shows the SiN_x etching profile the line with 300 nm line width and holes with 300 nm in diameter. The vertical profile is obtained by controlling the etching time. After removing the residual PMMA, the pattern was transferred into the InGaAsP MQWs layers by ICP etching at 160℃ with N_2:6 (sccm), Cl_2:5 (sccm), RF power:100(W) , ICP power:400(W) and pressure: 10 mtorr. Figure 2-1.6 shows the InP etching profile of the line with 300 nm line width and holes with 500 nm in diameter. The selectivity is about 9 for the photonic crystal patterns.

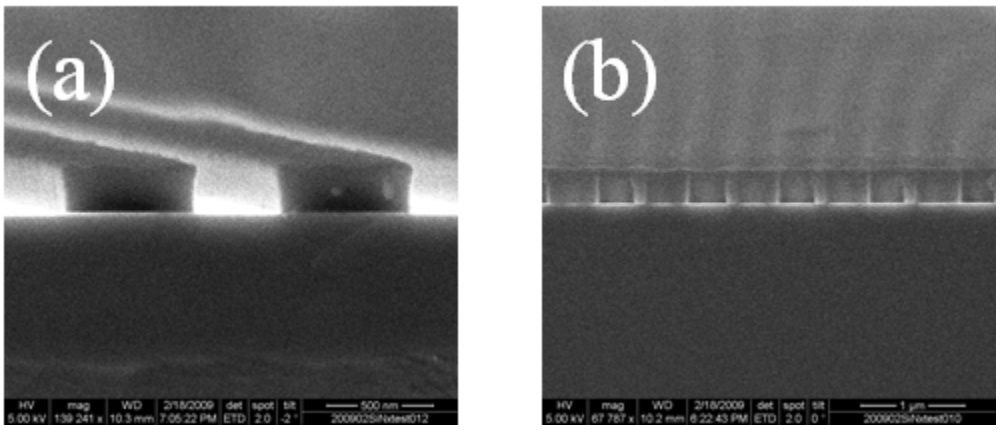

Figure 2-1.5 Cross section view for SiNx etching (a) grating (b) air hole

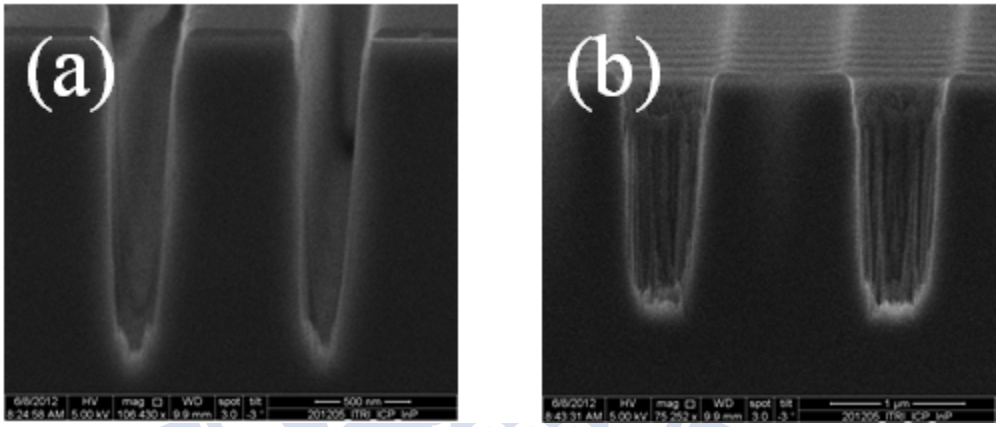

Figure 2-1.6 Cross section view for InP etching (a) grating (b) air hole

2-1-5 Wafer Bonding to PDMS substrate

Polydimethylsiloxane (PDMS) is a flexible elastomeric polymer that is commonly used in MEMS fabrication for a long time. It acts as a flexible substrate here, because it is optically clear and considered to be inert, non-toxic and non-flammable. We use the most common PDMS elastomers, Sylgard® 184 from Dow Corning®. Sylgard is a two part resin system containing vinyl groups (Part A) and hydrosiloxane groups (Part B). Mixing the two resin components together leads to a cross-linked network of dimethyl siloxane groups. We mix the A and B solutions with a 4:1 ratio of volumes. The ratio of A and B affects the hardness of the PDMS substrate. As the ratio becomes larger, the PDMS will be softer. It takes about 1 day that the mixed solution can be stiffening at 25℃. The volume of the PDMS glue we added controls the PDMS thickness. The refractive index of the PDMS is about 1.43, which can support good light confinement in the vertical laser structure.

With a well-prepared PDMS substrate, we can put the InP-etched device upside down and directly bond the two surfaces. After bonding the device to the PDMS substrate, diluted HCl solution (HCl: H_2O=2:1) is used to remove the InP substrate at room temperature for 60 minutes. The PDMS would not be destroyed during the wet etching process because it can afford strong acid and base.

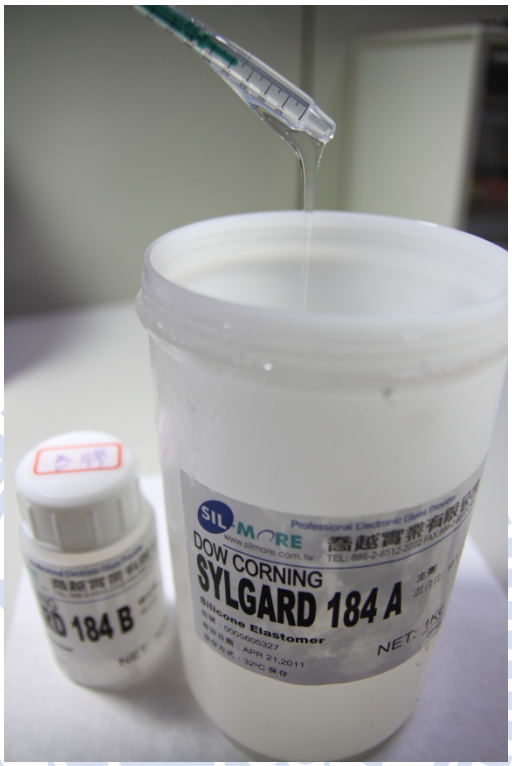

Figure 2-1.7 Sylgard® 184 A and B from Dow Corning®

2-2 Fabrication Steps for Flexible Photonic Crystal Rods Laser

The flexible photonic crystal rods in square-lattice were fabricated on a polydimethylsiloxane (PDMS) substrate. Figure 2-2.1 shows the partial illustration of the device structure. The accurate dimension of the device is 30×30 um^2. In fabrication, the epitaxial structure consisted of four 10 nm compressively strained InGaAsP multi-quantum-wells (MQWs) with 240 nm thickness which was grown on InP substrate is prepared. Figure 2-2.2 shows the epitaxial structure of InGaAsP/InP MQWs. It has been confirmed that the photo-luminance (PL) spectrum of the QWs is centered at 1550 nm and the full-width half-maximum (FWHM) is about 200 nm. The PL spectrum is shown in figure 2-2.3.

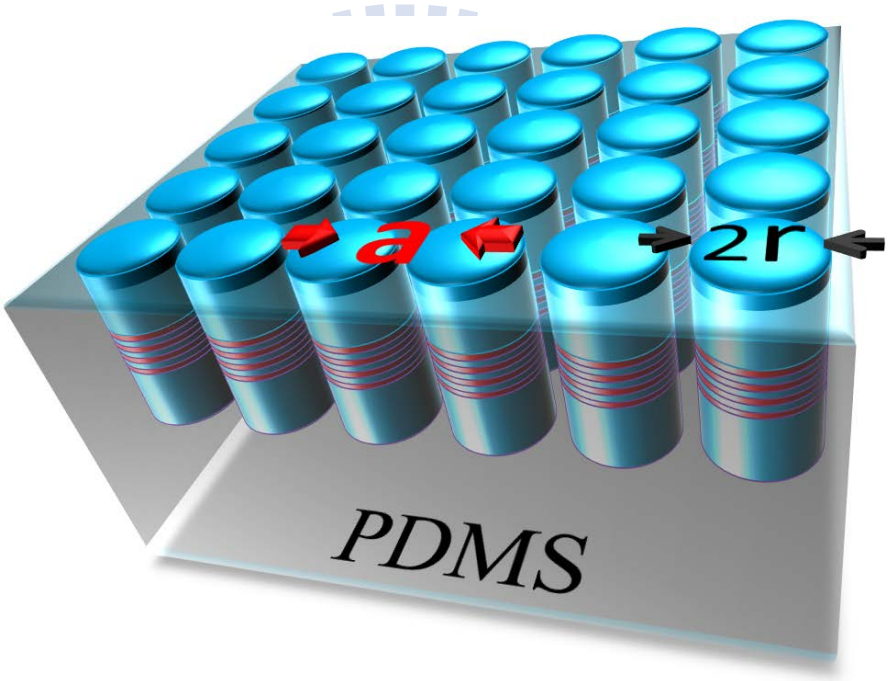

Figure 2-2.1 Illustration of the flexible photonic crystal square-lattice rods laser device structure

The PDMS substrate with a 250 um thickness takes the role of the flexible platform in our study. The refractive index of the PDMS is about 1.43, which is low enough to support good optical confinement in the vertical direction of the laser.

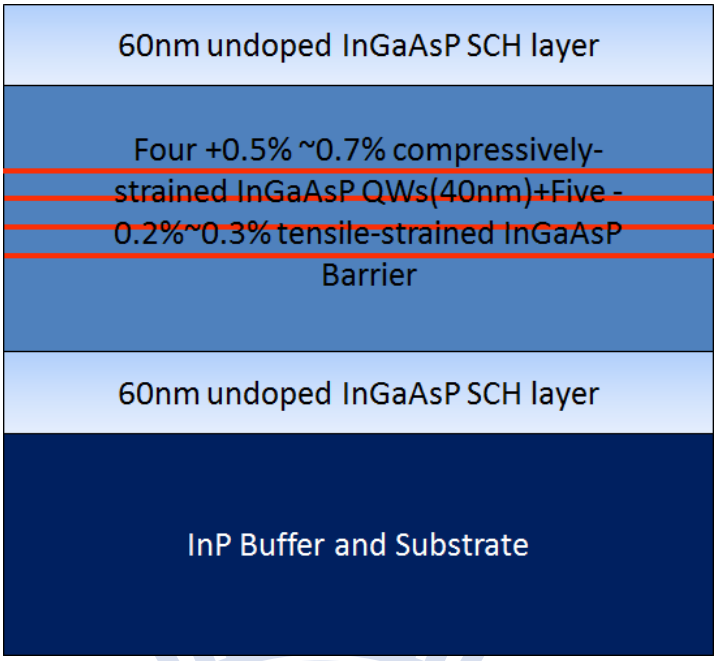

Figure 2-2.2 The epitaxial structure of InGaAsP QWs.

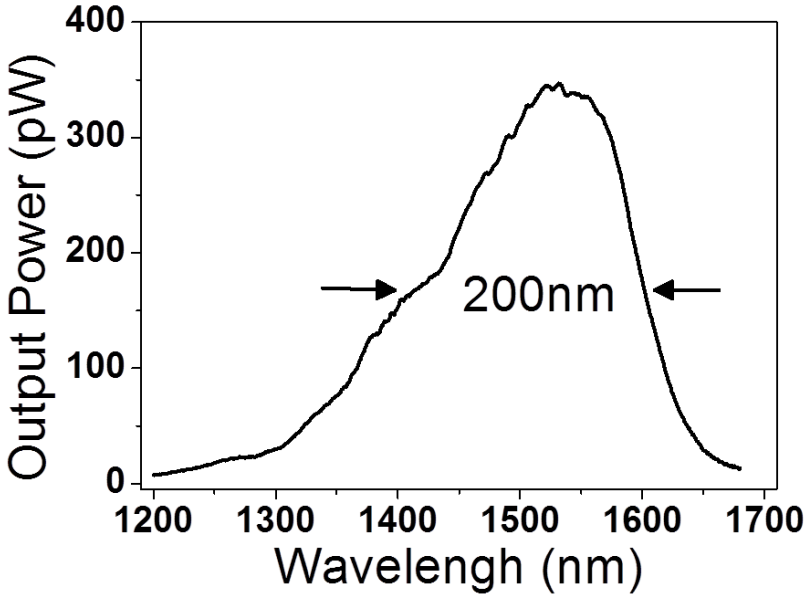

Figure 2-2.3 The PL spectrum of the InGaAsP/InP MQWs.

The silicon nitride layer as hard mask and the PMMA resist layer for defining photonic crystal rods were deposited and spin-coated on the QWs in sequence. The PC rods were defined by E-beam lithography on the PMMA resist layer. The lattice constant varies from 680 nm to 750 nm. After a series of RIE and ICP dry-etching processes, the patterns were transferred to the SiN_x layer with CHF_3/O_2 mixture gases at 20℃ and further to the QWs layer with N_2/Cl_2 mixture gases at 160℃. Thus we had made our laser structure on the InGaAsP layer. And then, the InGaAsP layer was put upside down and directly bonded on the

well-prepared PDMS substrate. Finally, the diluted HCl wet-etching process was introduced to remove the InP substrate. Therefore, the flexible photonic crystal rods laser device was formed after these steps. Figure 2-2.4 is the picture of the fabricated structure on a PDMS substrate.

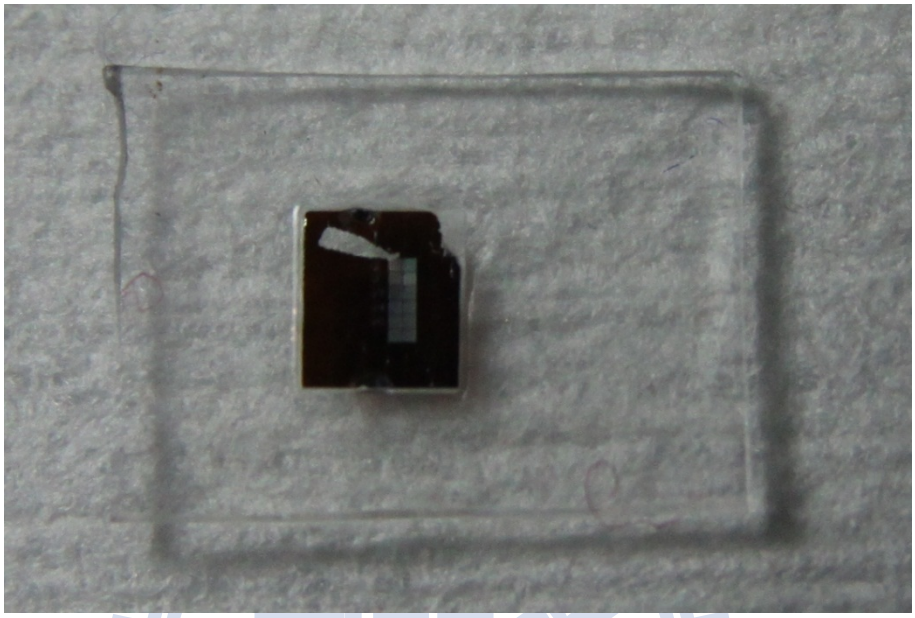

Figure 2-2.4 The picture of the fabricated structure on a PDMS substrate.

The flow chart of fabrication is shown below:

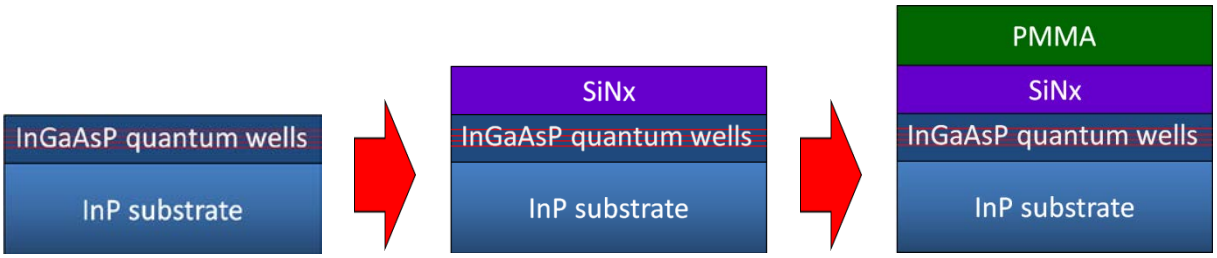

The InGaAsP wafer on InP substrate consists of 4 QW layers

SiN_x is deposited as hard mask layer.

PMMA layer is spin-coated as E-beam resist.

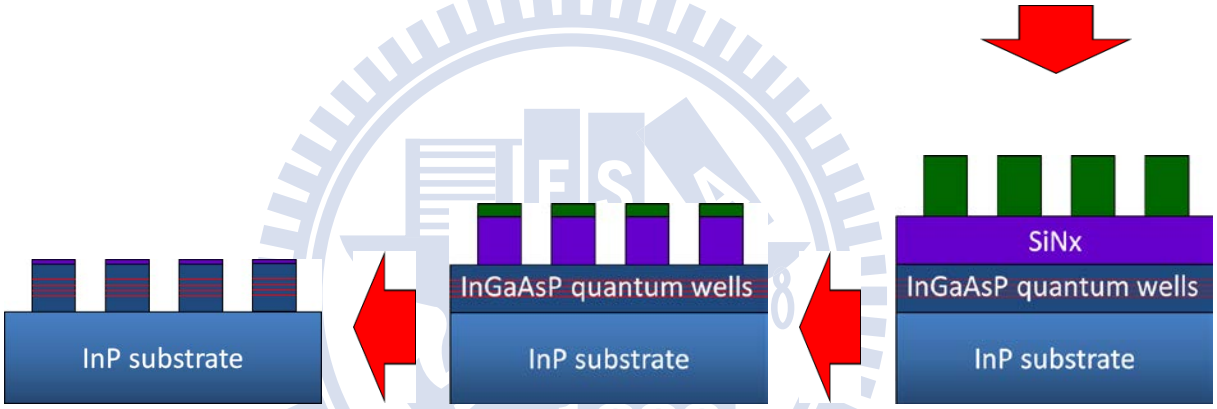

Transfer the patterns to InGaAsP layer by ICP.

Transfer the patterns to SiNx layer by RIE.

Define the patterns by E-beam lithography.

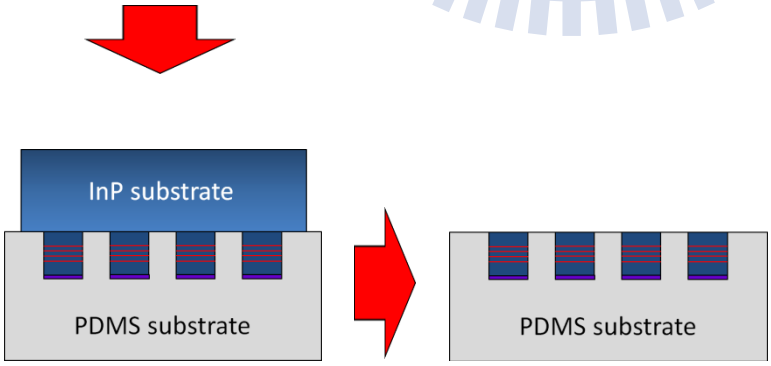

Wafer bonding to the the PDMS substrate.

Remove the InP substrate by wet-etching process.

2-3 Micro-PL Measurement Setups

In order to measure the optical properties of the photonic crystal micro-cavities, the micro-PL measurement system with sub-micrometer scale resolution in space and sub-nanometer scale resolution in spectrum is necessary. Figure 3-1.1 shows the micro-PL measurement system.

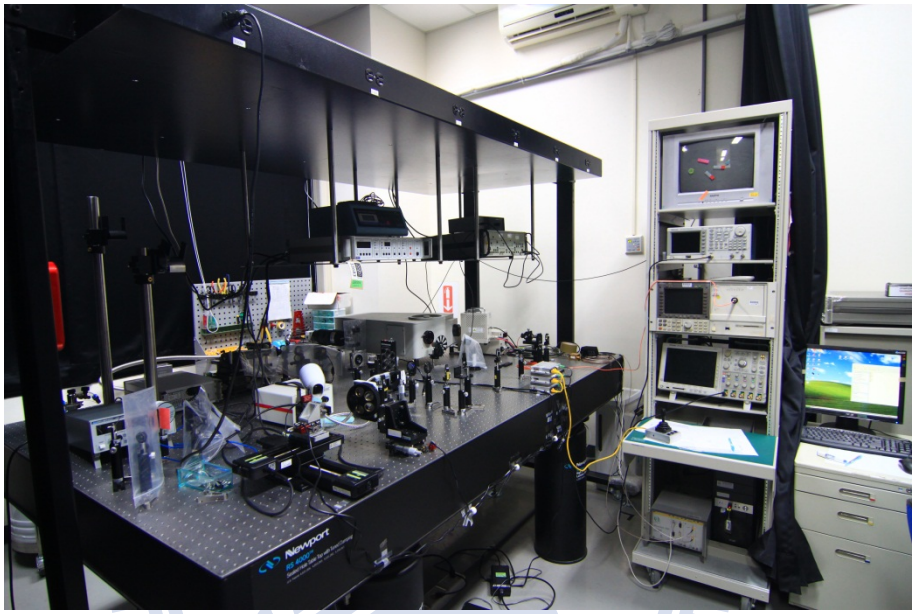

Figure 2-3.1 Picture of micro-PL measurement system

In the measurement system, the 850 nm diode laser is used as the pump source. The pump power is modulated by the amplitude modulator. The laser light goes through the 50/50 beam splitter, 50% of pump power is reflected into the photo-detector to know how much pump power that is used and the other 50% pump power is focused to a spot with 1.5 um to 2 um in diameter by the 100x NIR objective lens. The sample is mounted on a high resolution motor control 3-axis stage with 30 nm move resolution. The output power was collected from the top of the sample into the optical spectrum analyzer (OSA) by the objective lens, collective lens and multi-mode fiber. Because the most of the photonic crystal devices are only few um or sub-um scale, here we have to use the visible light system to observe the position of the pump spot and devices. The visible light system includes the visible light sources, CCD camera and monitor.

2-4 Conclusions

In this chapter, we have introduced the detailed fabrication process of the flexible photonic crystal rods laser device, including the utilized instruments and recipes in each step. With the well-tuned recipe, we can successfully fabricate the laser device, and the SEM image of the device is also shown above.

Chapter 3

Lasing Characteristics of Photonic Crystal Square Lattice Nanorods

In this chapter, we will show the photonic crystal square-lattice rods laser on a PDMS substrate. In order to identify the lasing mode, 2-D plane-wave-expansion (PWE) method and 3-D finite-element method (FEM) are introduced to calculate the optical mode. And then we bend the flexible substrate, comparing the laser characteristics to triangular holes lattice which was demonstrated in our previous work.

3-1 Lasing Performance on Flat PDMS Substrate

In chapter 2, we have shown the detailed fabrication process. Figure 3-1.1 is the SEM image of a field size on the fabricated device. A field size consists of 5×5 array and each column in the array have different lattice constant which was varied from 680 nm to 800 nm. Figure 3-1.2(a) shows the illustration of laser pumping position and photonic crystal square-lattice rods device on a PDMS substrate with 705 nm lattice constant and 0.37 r/a ratio. The dimension of a single device is 30×30 (um^2), resulting in about 40 period in both vertical and lateral sides. Figure 2-1.2(b) is the zoom-in SEM image of the laser device.

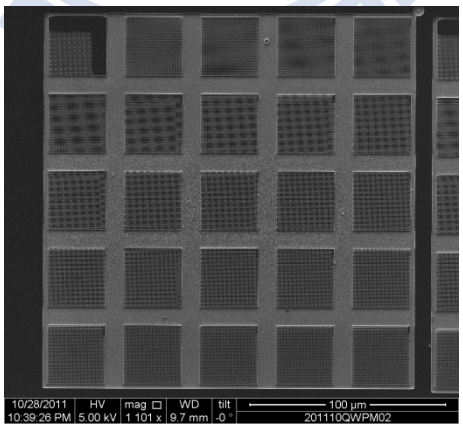

Figure 3-1.1 The SEM image of a field size consists of 5×5 array with different lattice constant.

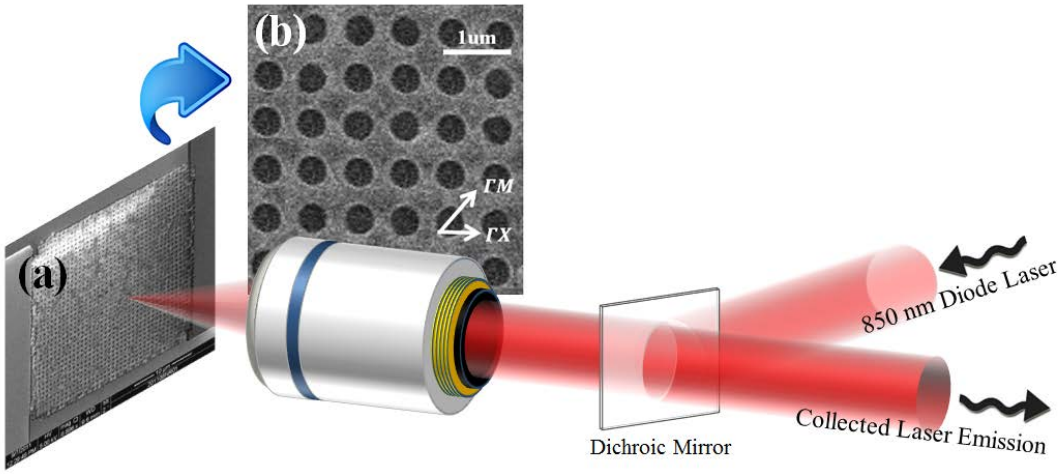

Figure 3-1.2 (a) Pumping spot is converged to focus on the center of the photonic crystal square-lattice rods structure on flexible PDMS substrate. (b) The zoom-in SEM image of photonic crystal square-lattice rods structure with 705 nm lattice constant and 0.37 r/a ratio.

3-1.1 Measurement Result

With a fabricated device on a flexible PDMS substrate, we measured the PL spectrum of MQWs at first. As shown in figure 3-1.3, the gain peak is around 1580 nm. There is a red-shift of 30 nm comparing to MQWs on InP substrate. The red-shift behavior is attributed to extremely low heat-conductivity of PDMS substrate. Heat accumulation result in high density of carriers and make the corresponding wavelength red shift. However, the full-width half-maximum (FWHM) of 150 nm from 1470 nm to 1620 nm is remained around 1.55 um. Still the lasing around communication wavelength could be expected.

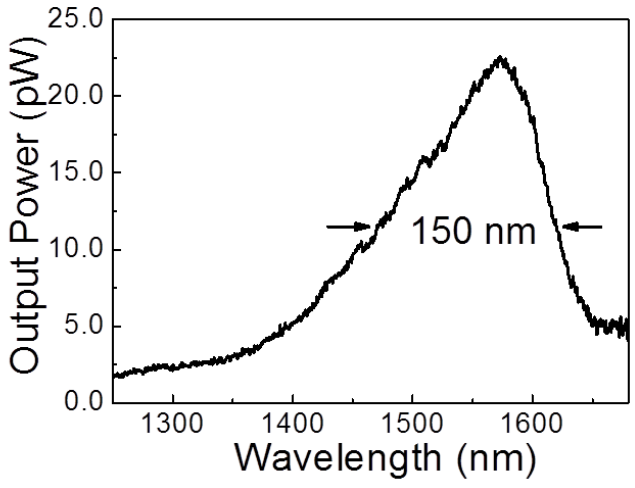

Figure 3-1.3 PL spectrum of MQWs on flexible PDMS substrate.

Figure 3-1.4 shows the lasing spectrum from photonic crystal square-lattice rods structure with 705 nm lattice constant and r/a ratio of 0.37. Under a pumping power of 0.8 mW, we observed that a single lasing mode is achieved at about 1600.4 nm. For the application of optical communication, the lasing peak supports high enough Side-mode Suppression-ratio (SMSR) of 23 dB.

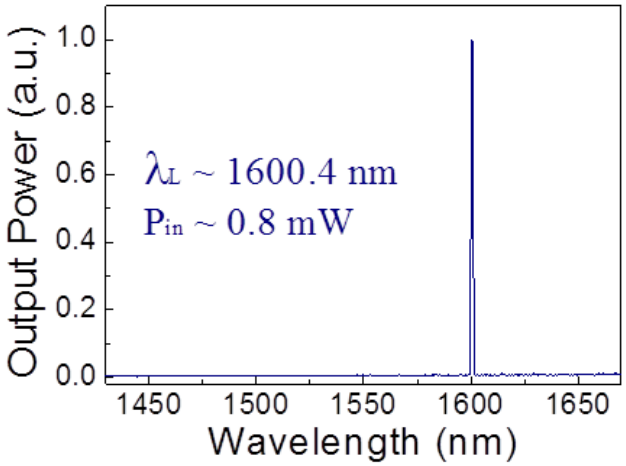

Figure 3-1.4 Lasing spectrum from photonic crystal square-lattice rods structure with 705 nm lattice constant.

From the Light-in & Light-out curve (L-L curve) shown in Figure 3-1.5, we could observe linear behavior after turn-on. It indicates the laser action and the threshold power is about 0.59 mW. We also measured the linewidth around threshold power. The narrowing linewidth shows the transition from spontaneous emission to stimulated emission of the optical mode. The Q factor of cold cavity is estimated about 7500 by wavelength to linewidth around transparency.

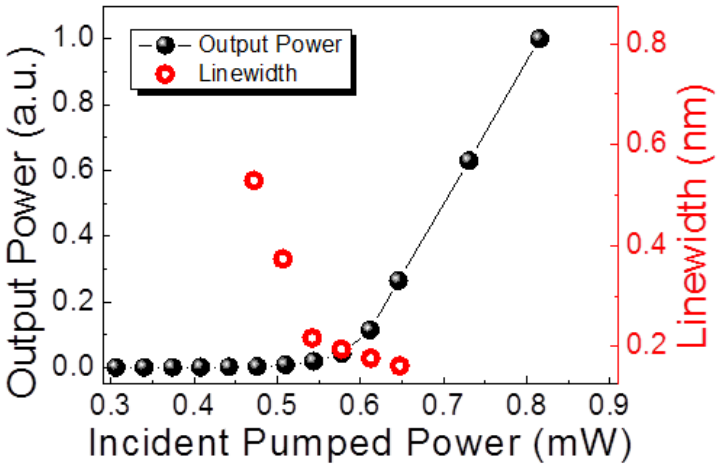

Figure 3-1.5 Light in & Light out curve (L-L curve) and Linewidth of the lasing peak.

For photonic crystals, the wavelength is relative to parameters of lattice constant, r/a ratio and refractive index of materials…etc. In order to identify the operation mode of the photonic crystal rods laser, we measured the other devices with different lattice constant in the same array. The devices in the same array would have the same r/a ratio. The measurement result is shown in figure 3-1.6, and we observe that the wavelength increases linearly as the lattice constant increases. The estimated normalized frequencies of different constant are all around 0.44 by lattice constant to wavelength. It indicates that the lasing mode should be the same mode.

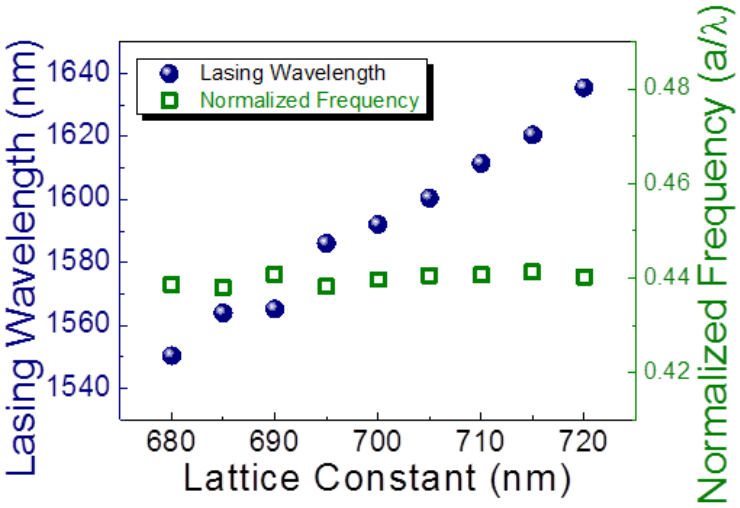

Figure 3-1.6 Lasing wavelength increases as the lattice constant increases. The normalized frequency is estimated around 0.44.

3-1.2 Photonic Crystal Band-edge Mode

For the photonic crystal square-lattice rods laser structure with r/a ratio of 0.37, the corresponding band structure for TE-like is obtained by 2-D plane-wave-expansion (PWE) method to extinguish the optical mode, as shown in Figure 3-1.7. In general, the photonic crystal band-edge modes are likely to occur around high-symmetry points of the band structure, and utilizing the flat photonic band with low group velocity to enhance the light-gain interaction. Therefore, the lasing action can be expected. As mentioned above, we have measured a lasing mode with the normalized frequency around 0.44, which is extremely close to the first band on Γ-point. Comparing the experimental and calculated results, we identify that the Γ_1 point in the band structure is the operation mode of the photonic crystal rods laser.

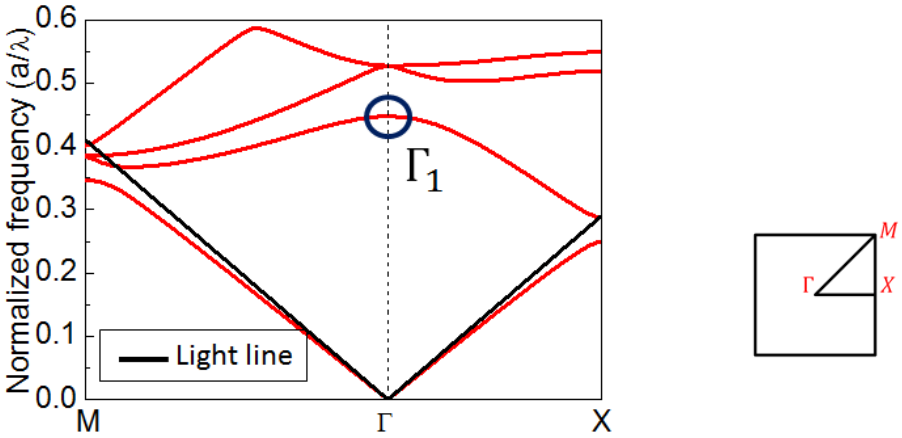

Figure 3-1.7 2-D PWE simulated TE-like band structure of the photonic crystal square-lattice structure.

From the band structure, we can observe that k-path of the Γ-point modes is zero on the high symmetry point, and the low curvature of the band results in low group velocity. Furthermore, the position of Γ_1 is in the band gap of the X symmetry point, establishing confinement of Γ-X direction. These evidences indicate Γ_1 is a strongly localized mode. On the other hand, the Γ_1 mode couples with another two modes. One is the waveguided modes through their k-vector components in the second, third Brillouin zone and further more. Secondly, the Γ_1 point is far away from light line, as we know modes above light line are radiated modes, resulting in light leakage into air. This is why the Q factor of 7500 we measured is lower than general photonic crystal defect lasers which have small mode volume. But most of all, coupling to radiated mode allows the opening to free space, making the device as a high-output power surface emitting laser.

In addition, we perform 3-D finite-element method (FEM) simulation to confirm the operation mode. The simulation model consists of InGaAsP rods and PDMS layer, and the refractive indices are 3.4 and 1.437, respectively. We calculate the structure for H_z field of TE mode. Figure 3-1.8 shows the simulated optical mode profile of the photonic crystal square-lattice rods laser with 705 nm lattice constant and r/a ratio of 0.37. The wavelength is around 1613 nm, which has some difference comparing to experimental result. We attribute the difference to fabrication inaccuracies. From the mode profile, we can observe that the field intensity of both lateral and vertical profile is strongly localized in the InGaAsP rods. The simulated result could agree with the 2-D PWE simulation we demonstrated above. For convenience and consistency, we will perform 3-D FEM simulation to figure out the experimental data in sequence.

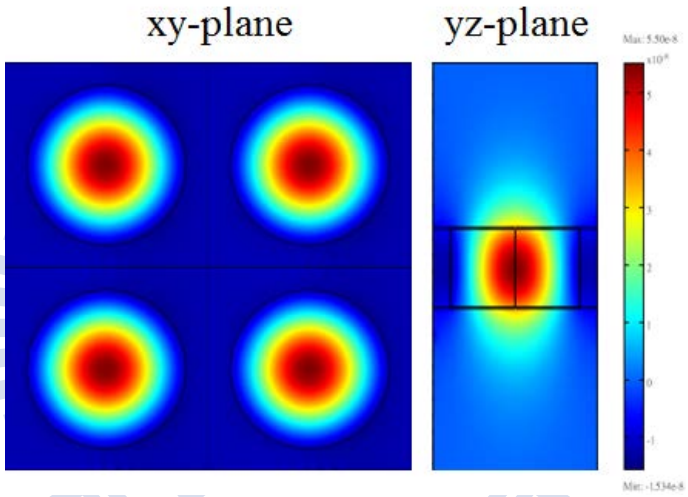

Figure 3-1.8 Optical mode profile calculated for H_z field of TE mode by 3-D FEM simulation.

3-2 Lasing Characterization with Different r/a Ratio

After identifying the operation mode of the photonic crystal square-lattice rods laser, we try to analyze the properties of laser with several tuned parameters. First we define the device A to F from higher r/a ratio to lower r/a ratio. In the same pumping condition, these devices do achieve lasing, but device A is excluded. Figure 3-2.1 shows the lasing spectrum of devices in different r/a ratio but the same lattice constant of 705 nm, thus the wavelength shift totally depends on the r/a ratio. We can observe that the lasing wavelength decreases as r/a ratio decreases because the corresponding normalized frequency decreases as shown in Figure 3-2.2. In the 2-D photonic crystal membrane, the effective index decreases as r/a ratio decreases, causing the normalized frequency dropped and lasing wavelength blue-shifted.

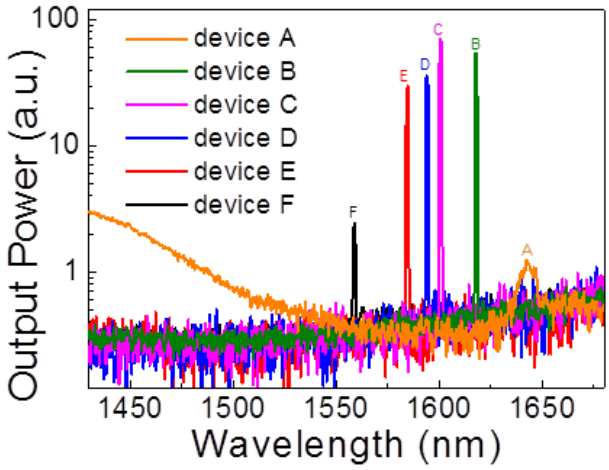

Figure 3-2.1 Lasing spectrum from devices of different r/a ratio in the same lattice constant of 705 nm.

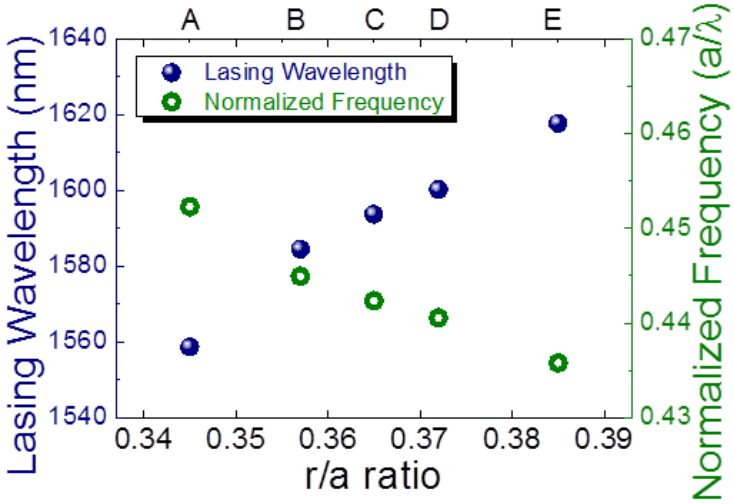

Figure 3-2.2 Lasing wavelength and corresponding normalized frequency of devices A to E with different r/a ratio.

What we concern about most in the devices of different r/a ratio is how r/a ratio affect the laser characterization. The variation of threshold power and quality factor are shown in Figure 3-2.3. For the period of r/a ratio between 0.34 and 0.39, we can find out that as the r/a ratio increases, the pumped effective power density decreases, and the quality factor increases as the r/a ratio increases. An increase of 60% in quality factor and a drop of 10% in pumped effective power density are observed. In a device with higher r/a ratio, the rods take the larger dimension in a unit cell, allowing more gain to support lasing action. On the other hand, the rods get closer to each other with higher r/a ratio; hence the communication between rods gets stronger. The rise in quality factor is attributed to these two reasons, and results in the drop of pumped effective power density.

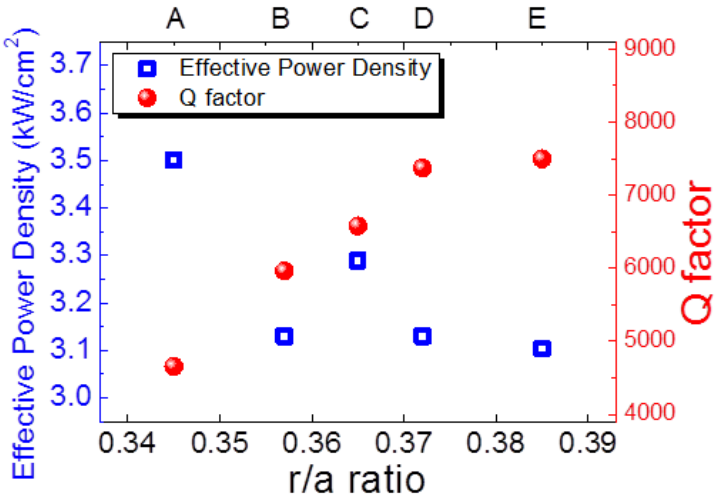

Figure 3-2.3 Variation of pumped effective power density and quality factor with different r/a ratio in 705 nm lattice constant.

Following a 3-D FEM simulation for wavelength variation in different r/a ratio and 705 nm lattice constant is performed to fit the experimental result. The wavelength has a linearly red-shift trend when r/a ratio become larger as shown in Figure 3-2.4. The lasing wavelength in experiment is also marked and the difference between experiment and simulation is due to fabrication inaccuracy. In summary, the simulation result agrees with the experimental data.

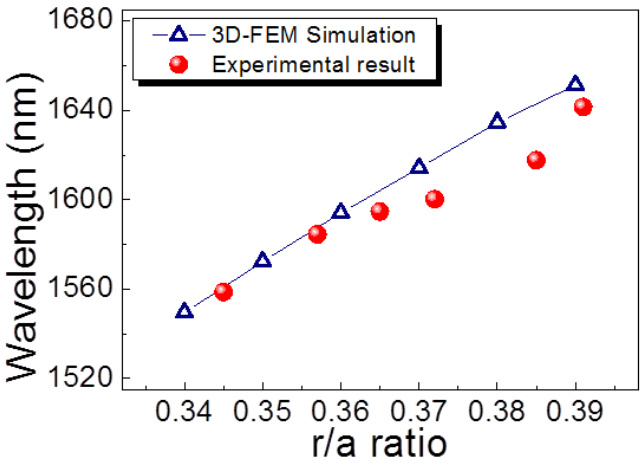

Figure 3-2.4 Simulation result for wavelength variation in different r/a ratio and lattice constant of 705 nm. Experimental result is also marked.

3-3 Conclusions

In this chapter, we demonstrate the photonic crystal square-lattice rods laser on a flexible PDMS substrate. The lasing modes are observed with different lattice constant and the normalized frequency of 0.44 is confirmed. Both the result of 2-D PWE method simulation and 3-D FEM simulation we performed could agree with the experimental data. Also the lasing characterization with different r/a ratio is shown in this chapter.

Chapter 4

Lasing Characteristics on Flexible Platform

In this chapter, a homemade stage is introduced to serve as the lattice extending platform. With the stage, we demonstrate the lasing characterization with different lattice extension percentage along both Γ-X direction and Γ-M direction. The 3-D FEM simulation is also performed to identify the variation trend of lasing wavelength.

4-1 Calibration of Lattice Extension Percentage

In our previous work, a multi-wavelength photonic crystal band-edge laser in triangular hole-lattice on a flexible PDMS substrate was demonstrated [24]. We have shown the illustration of the bent photonic crystal triangular hole-lattice laser structure with bending radius R in Figure 1-2.1. The structure could be bent by a handmade bending tool. As the bending curvature increases, the InGaAsP membrane on PDMS substrate is strained; hence the lasing property is altered and the wavelength red-shifts due to lattice deformation.

However, the InGaAsP membrane was regarded as the main factor for limiting the tuning range of wavelength in this bending system. It's because InGaAsP membrane has much higher Young's modulus than flexible PDMS substrate. We can't successfully extend the triangular hole-lattice with strong strains of InGaAsP membrane. In order to eliminate the strains from hard InGaAsP membrane, the photonic crystal square-lattice rods structure is introduced to this multi-wavelength tuning system. The rods structure was directly embedded to flexible PDMS substrate and each rod had no connection with neighboring rods. On the other hand, the bending stage we used ran into bottom necks on larger bending curvature. As a result we bring in an extending platform to directly extend the lattice of photonic crystal structure in horizontal direction. Hence the lattice constant can be easily extended for larger lattice variation; a much wider tuning range in lasing wavelength could be expected.

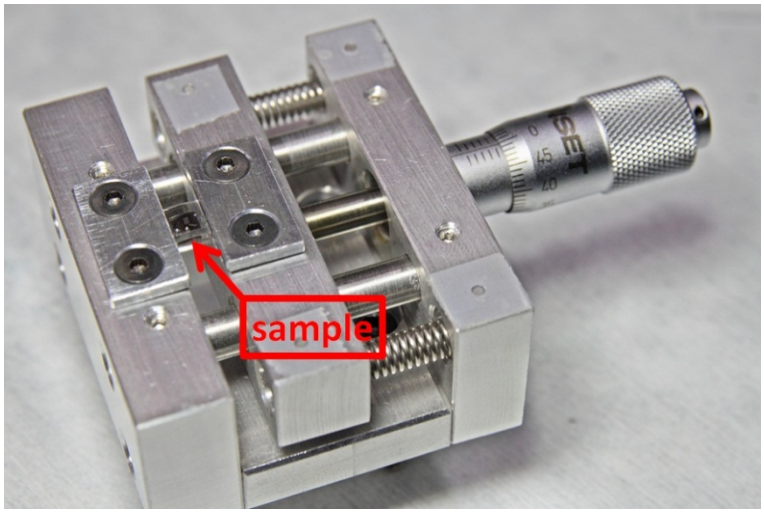

Figure 4-1.1 Image of the homemade stage which serves as the extending platform. Sample is fixed on the stage by two clamps and extended by rotating the micrometer.

Figure 4-1.1 shows the picture of homemade extending stage. Sample is fixed on the stage by two clamps as shown in Figure 4-1.2. The distance between two straight red lines indicate the original length of 5 mm before being extended. By rotating the micrometer, the sample could be extended in lateral direction. We estimate the lattice extension percentage by variation of length to original length.

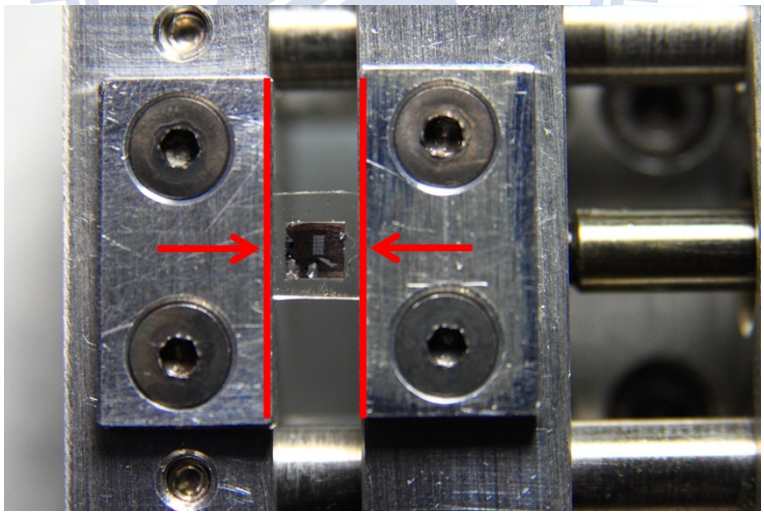

Figure 4-1.2 Zoom-in picture of sample on the homemade extending stage. The distance between two red lines is 5 mm.

As mentioned in chapter 2, our photonic crystal square-lattice rods structure was fabricated on hard InGaAsP layer and then bonded to soft PDMS substrate. There are some native differences among the two materials, including Young's modulus and Poisson's ratio. When we extend the photonic crystal square-lattice rods structure, nonuniform strains might

lead to various variations of InGaAsP layer and PDMS substrate. As a result, calibration of the accurate lattice extension percentage is needed in this lattice extending system.

First of all, we want to make sure whether the lattice extension percentage is uniform in the whole patterned area. Figure 4-1.3 shows the SEM picture of a fabricated device on PDMS substrate; five areas in a large dimension of 1200×400 um^2 were chosen to process calibration and were defined from A to E, respectively. The dimension of area A, C and E are 200×200 um^2 and area B and D are a single device of 30×30 um^2 in dimension. Following we measured the variation of length in each area using SEM as the sample was extended step by step. The accurate lattice extension percentage of each area versus rotated distance of micrometer and variation in length of the device were plotted in Figure 4-1.4. ΔR indicates rotated distance of micrometer, and ΔX is the corresponding increased distance in lateral direction. By dividing ΔX to X, we call the ΔX/X ratio as sample extension percentage. We can find that the variation of lattice extension percentage is approximately linear of each area when sample extension percentage increases to 15 %, and the average slop is about 0.74 (%/%), which indicates an equivalent lattice extension percentage of 0.74 % could be reached by increasing the sample extension percentage for 1 %.

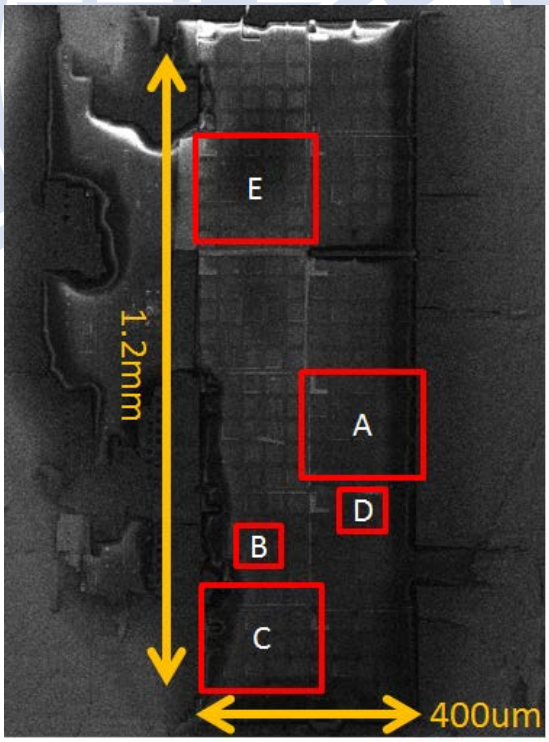

Figure 4-1.3 SEM picture of calibrated sample. Marked areas were measured and the corresponding extension percentages were calculated by variation of length to original length.

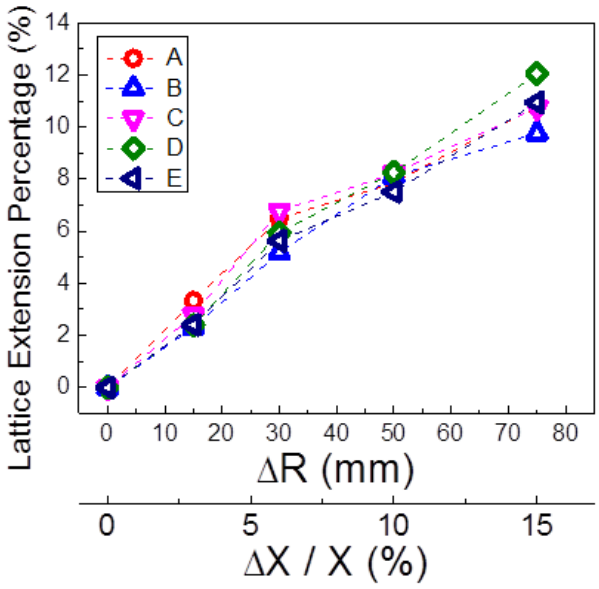

Figure 4-1.4 Lattice extension percentage versus ΔR and ΔX/X. ΔR is rotated distance of micrometer, and ΔX /X is the corresponding sample extension percentage.

4-2 Lasing Characteristics of Photonic Crystal Lattice Extended along Γ-X Direction

As mentioned in chapter 2, the operation lasing mode is strongly localized in the InGaAsP rods. This feature implies that the lasing characteristics might depend on its designed geometry. That's why we fabricated the laser structure on flexible PDMS substrate, because the geometry of the laser structure could be fine-tuned easily and the lasing wavelength could be manipulated when the photonic crystal lattices are extended in the flexible PDMS substrate. First we measured the lattice extended device along Γ-X direction. Figure 4-2.1 shows the illustration of extended photonic crystal square-lattice rods structure along Γ-X direction. The flexible device is fixed by two clamps and the two arrows stand for the lattice extended direction.

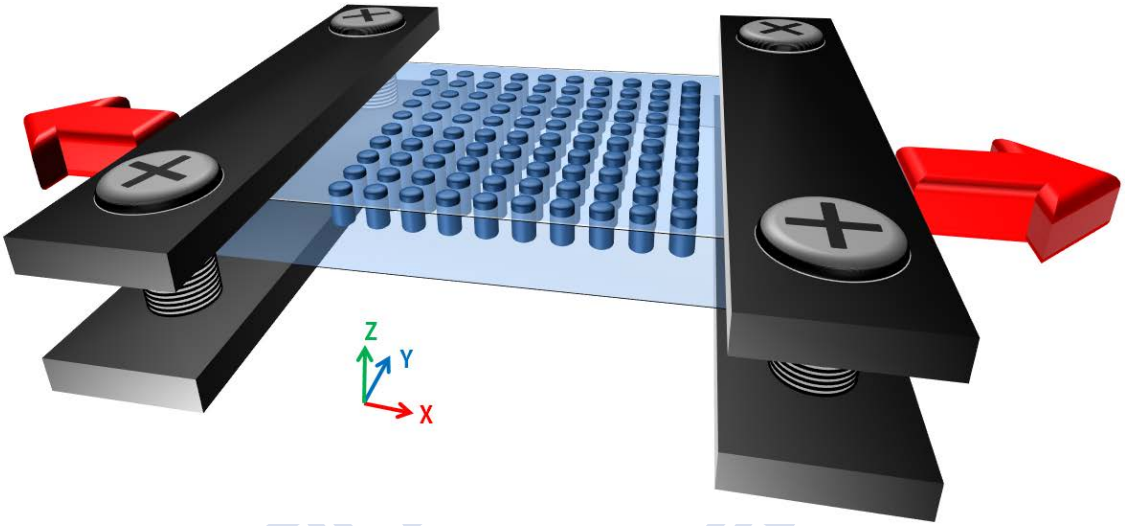

Figure 4-2.1 Illustration of lattice extended along Γ-X direction

4-2.1 Experimental Results

We measure device C with 705 nm lattice constant. Figure 4-2.2 shows the light-in & light-out curve (L-L curve) of the laser with different lattice extension percentage. The structure does achieve lasing at varied lattice extension percentage. The lasing spectrum with different lattice extension percentage were recorded and plotted in Figure 4-2.3. We could find that the lasing peak was altered as the lattice extension percentage increased. It implies that the laser could be applied as a wavelength tunable laser light source in optical communication. Finally the lasing peak vanished and became a resonance with the lattice extension percentage of 10.36 %.

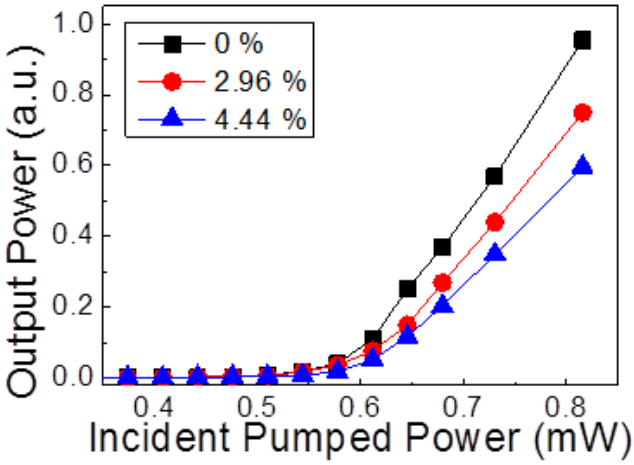

Figure 4-2.2 Light-in & light-out curve of the 705 nm flexible photonic crystal square-lattice rods laser with different lattice extension percentage along Γ-X direction.

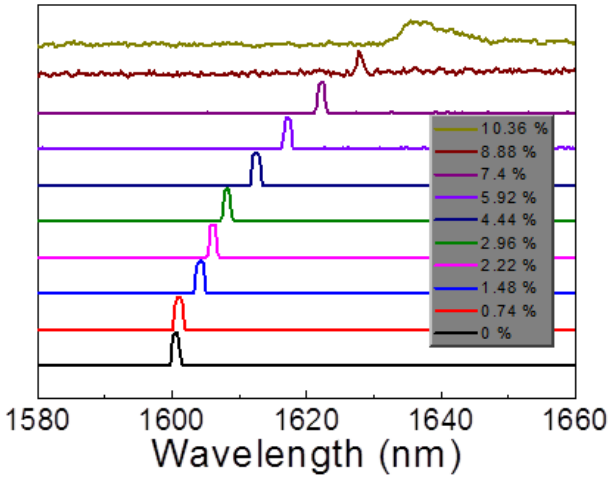

Figure 4-2.3 Lasing spectrum of the 705 nm lattice constant flexible photonic crystal square-lattice rods laser with different lattice extension percentage along Γ-X direction.

The lasing wavelength and resonant wavelength of the photonic crystal square-lattice rods laser with different lattice extension constant are shown in Figure 4-2.4. We observe that the wavelength increase linearly with the extension ratio of photonic crystal lattices. Within the lattice extension percentage from zero to 8.88 %, the lasing wavelength was shifted approximately 26.4 nm. In order to characterize the red-shift behavior in lasing wavelength, we define wavelength tunability as the ratio of variation of wavelength to lattice extension percentage. The lasing wavelength tunability of the flexible photonic crystal square-lattice rods laser is approximately 2.97 (nm/%). The red-shift behavior is attributed to small lattice distortion of photonic crystals on the flexible substrate.

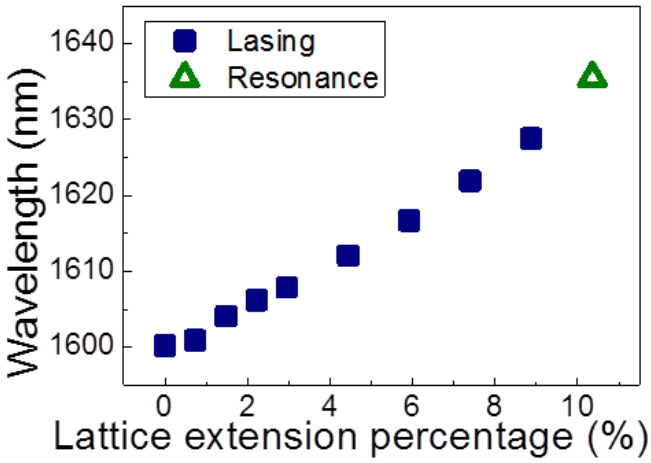

Figure 4-2.4 Lasing wavelength versus the lattice extension percentage along Γ-X direction of the 705 nm lattice constant flexible photonic crystal square-lattice rods laser.

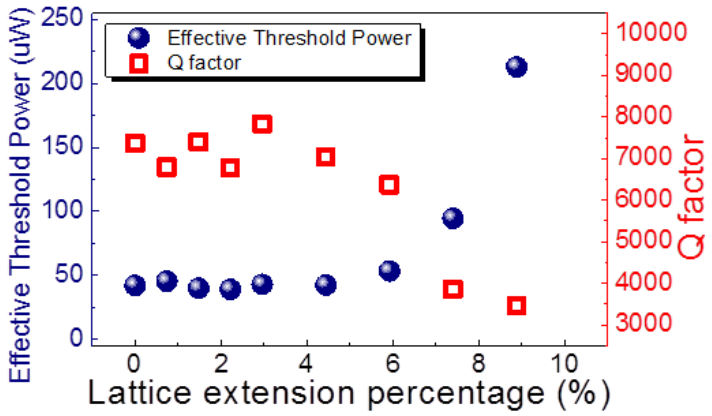

Figure 4-2.5 Effective threshold power and quality factor of the 705 nm lattice constant flexible photonic crystal square-lattice rods laser with different lattice extension percentage along Γ-X direction.

In the operation range of lattice extension percentage from zero to 8.88 %, an increase of 300 % in effective threshold power and a decrease of 50 % in quality factor are observed and shown in Figure 4-2.5. As the lattice extension percentage increases, each rod in the square-lattice structure is pulled away from neighboring rods. Less coupling efficiency of the localized mode in rods leads to drop in quality factor of the whole cavity. In addition, the mode volume also decreases when the photonic crystal lattices are extended. These features are considered to bring out the increase in effective threshold power.

4-2.2 Simulation Results

In our experiment with the lattice extension system, lattice extension is considered as the dominator in the variation of lasing wavelength. Figure 4-2.6 illustrates the model for the lattice variation. Lattice constant in horizontal Γ-X direction is extended and lattice constant in vertical Γ-X direction remains the same when the device is extended along horizontal Γ-X direction. The blue circles are the original lattices and brown circles in dash denote the extended lattices. For example, the 705 nm lattice constant will be extended to 846 nm with 20 % lattice extension percentage. Figure 4-2.7 is the illustration of a unit cell deviation when the lattice is extended. We take the varied unit cell into 3-D FEM simulation for TE mode and the simulated results are shown below.

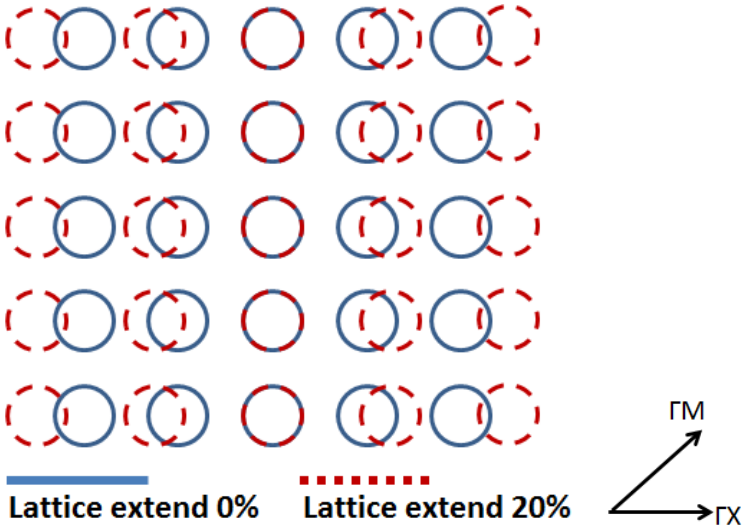

Figure 4-2.6 Illustration of our model for the lattice variation along Γ-X direction

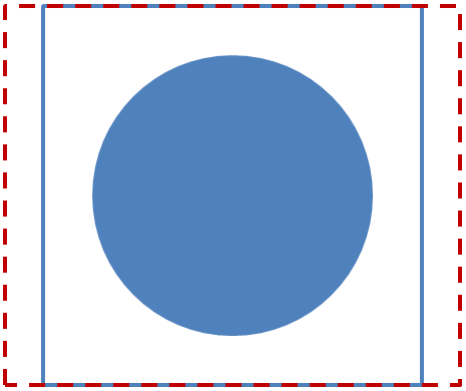

Figure 4-2.7 Illustration of a unit cell deviation of photonic crystal square-lattice rods structure with 20 % extended lattice along Γ-X direction

Figure 4-2.8 shows the Hz mode profiles for TE mode of photonic crystal rods laser with 705 nm lattice constant and r/a ratio of 0.37 in different lattice extension percentage of 0 %, 4 % and 10 % along Γ-X direction. When the lattice extended, the modes remain strongly localized in the rods instead of diverging into air, PDMS or lateral direction. It reveals that the photonic crystal square-lattice rods laser does not propagate along Γ-X direction in membrane and low group velocity in in-plane direction agrees with the lasing mode in Γ symmetry point.

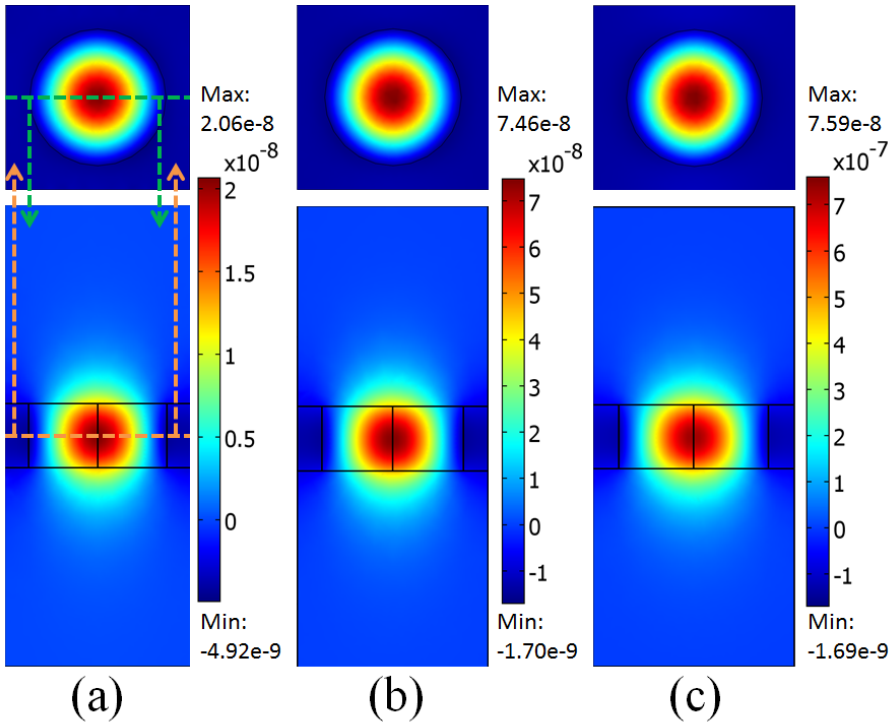

Figure 4-2.8 Mode profiles for TE mode in Hz field of photonic crystal square-lattice rods laser with 705 nm lattice constant in different lattice extension percentage along Γ-X direction. (a) Original un-extended square lattice (b) Lattice extension percentage of 4 % (c) Lattice extension percentage of 10 %

Comparing the experimental result to simulated result in 3-D FEM calculation, the red-shift behaviors of wavelength shown in Figure 4-2.9 are similar to each other. The simulated wavelength versus lattice extension percentage has a slop around 2.72 (nm/%) and the experimental wavelength versus lattice extension percentage has a slop around 2.97 (nm/%). However, the wavelength of experiment and simulation are not exactly the same but close. Both difference of wavelength peak and wavelength variation slop between experiment and simulation could be attributed to fabrication inaccuracy.

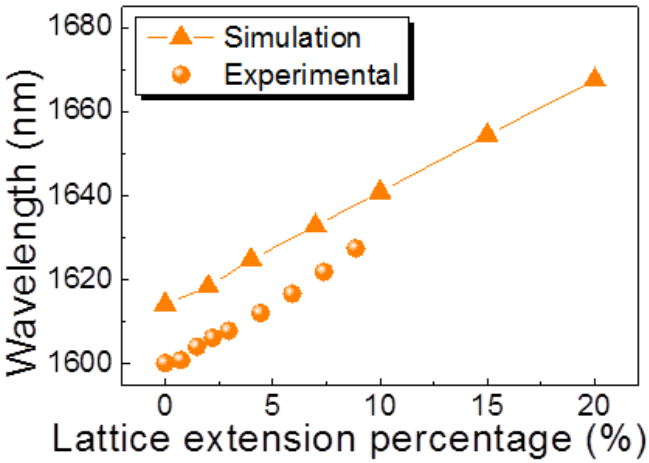

Figure 4-2.9 Comparison between experimental result and simulated result with extended lattice along Γ-X direction

In addition, device D and device E with 705 nm lattices constant were also measured and the variation in wavelength is plotted in Figure 4-2.10. The wavelength tunability of device D is around 2.76 (nm/%) and device E is 2.67 (nm/%). Navy blue symbols and lines are 3-D FEM simulation results with 705 nm lattice constant and varied r/a ratio from 0.34 to 0.39 in different lattice extension percentage.

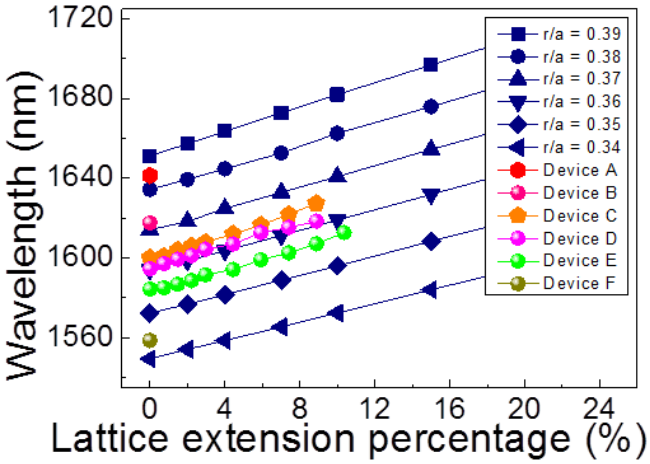

Figure 4-2.10 Comparison of wavelength tunability slop between experiment and simulation with varied r/a ratio.

4-3 Lasing Characteristics of Photonic Crystal Lattice Extended along Γ-M Direction

In the section 4-2, we demonstrated the operation lasing mode red-shift as lattice extension percentage increased. Both threshold power and quality factor were also changed. This feature implies that geometry of the laser cavity plays an important role for the lasing characteristics. As a result we are curious whether lattice extension along Γ-M direction affects the lasing characteristics. Figure 4-2.1 shows the illustration of extended photonic crystal square-lattice rods structure along Γ-M. The flexible device is rotated by 45 degrees and fixed by two clamps. The two arrows indicate the lattice extended direction.

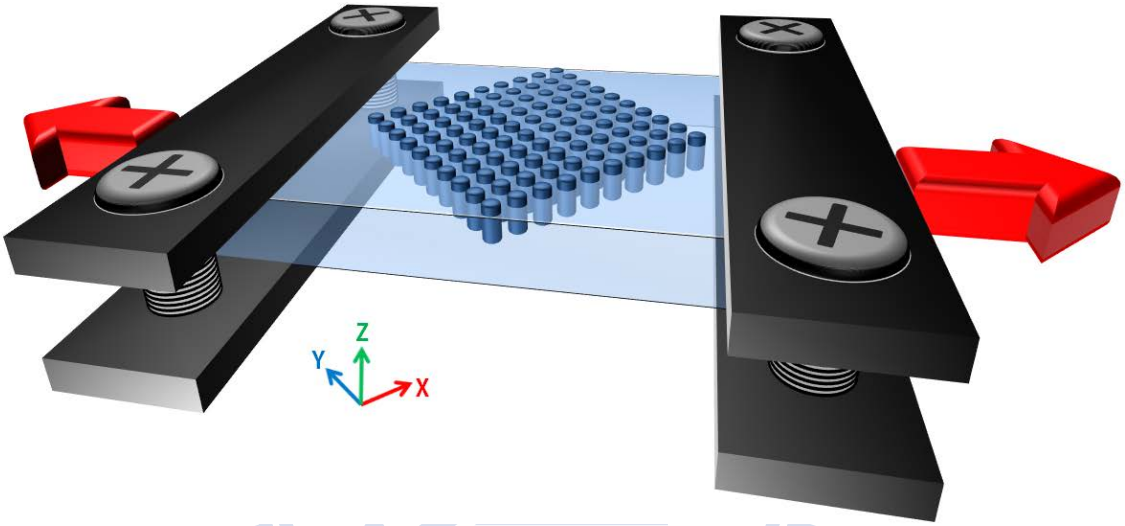

Figure 4-3.1 Illustration of lattice extended along Γ-M direction

4-3.1 Experimental Results

We measure device C with 705 nm lattice constant. Figure 4-3.2 shows the light-in & light-out curve (L-L curve) of the laser with different lattice extension percentage. The structure does achieve lasing at varied lattice extension percentage. The lasing spectrum with different lattice extension percentage from 0 % to 12.42 % were recorded and plotted in Figure 4-3.3. We could find out that the lasing peak was altered and red-shift like lattice extension along Γ-M direction as the lattice extension percentage increased.

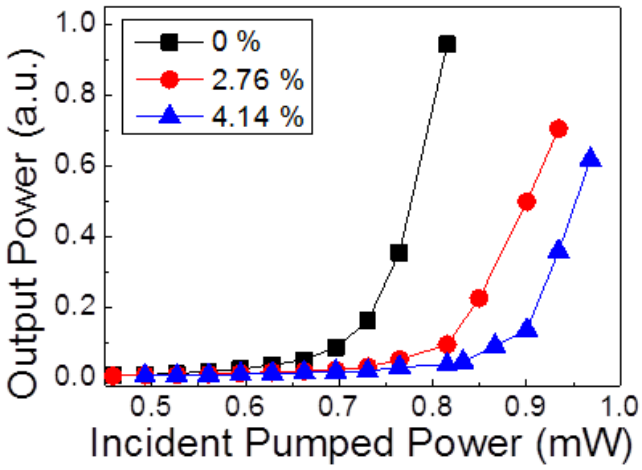

Figure 4-3.2 Light-in & light-out curve of the 705 nm photonic crystal square-lattice rods laser with different lattice extension percentage along Γ-M direction.

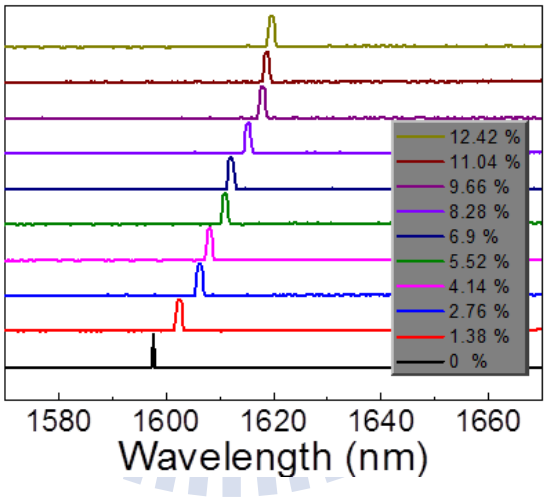

Figure 4-3.3 Lasing spectrum of the 705 nm photonic crystal square-lattice rods laser with different lattice extension percentage along Γ-M direction.

The lasing wavelength of the photonic crystal square-lattice rods laser with different lattice extension constant is shown in Figure 4-3.4. We observe that the wavelength increase linearly with the extension ratio of photonic crystal lattices. Within the lattice extension percentage from zero to 12.42 %, the lasing wavelength was shifted approximately 21.45 nm. The lasing wavelength tunability of the flexible photonic crystal square-lattice rods laser is approximately 1.72 (nm/%). Similar to lattice extension along Γ-X direction, the red-shift behavior is attributed to small lattice distortion of photonic crystals on the flexible substrate.

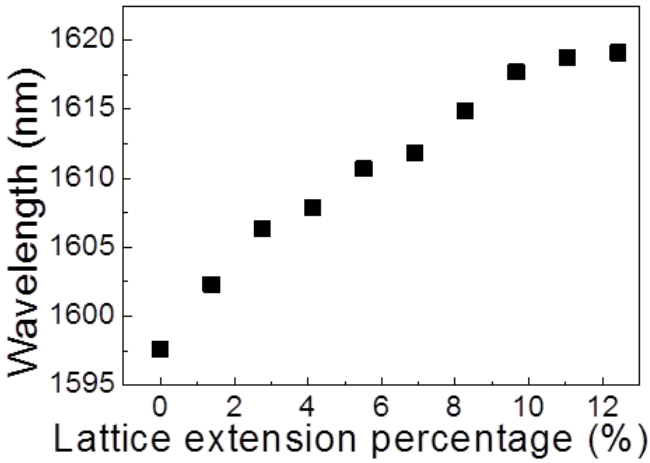

Figure 4-3.4 Lasing wavelength versus the lattice extension percentage along Γ-M direction of the 705 nm lattice constant photonic crystal square-lattice rods laser.

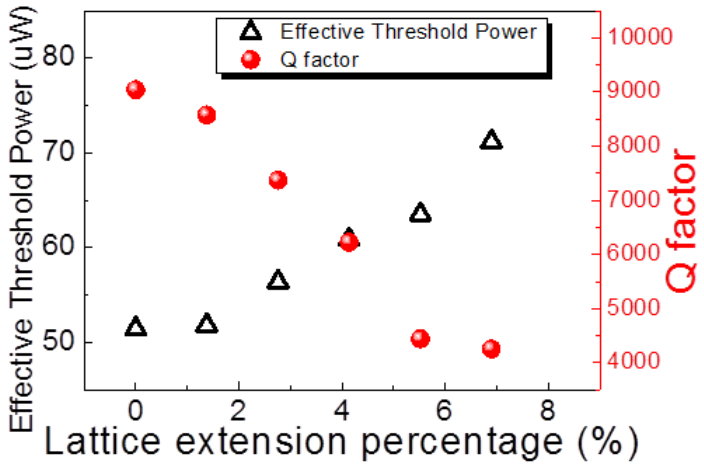

Figure 4-3.5 Effective threshold power and quality factor of the 705 nm lattice constant photonic crystal square-lattice rods laser with different lattice extension percentage along Γ-M direction.

In the operation range of lattice extension percentage from zero to 6.9 %, an increase of 40 % in effective threshold power and a decrease of 50 % in quality factor are observed and shown in Figure 4-3.5. These variation trends were similar to lattice extension along Γ-X direction and the same reason like lattice distortion and decreasing mode volume were considered affecting the lasing characterization.

4-3.2 Simulation Results

Figure 4-3.6 illustrates the model for the lattice variation. Lattice constant in horizontal Γ-M direction is extended and lattice constant in vertical Γ-M direction remains the same when the device is extended along horizontal Γ-M direction. The blue circles are the original lattices and brown circles in dash denote the extended lattices. Figure 4-3.7 is the illustration of a unit cell deviation when the lattice is extended. We take the varied unit cell into 3-D FEM simulation for TE mode and the simulated results are shown below.

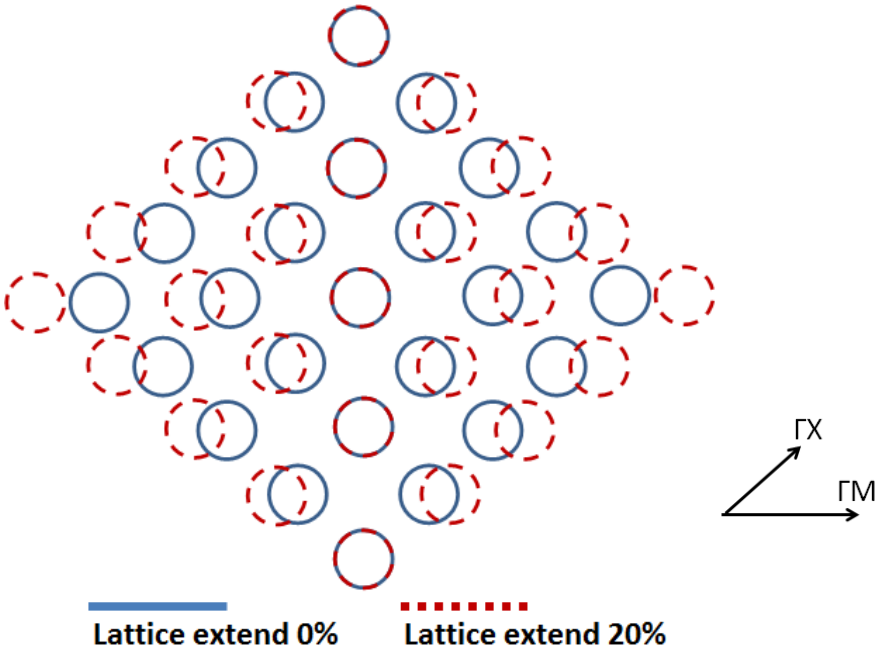

Figure 4-3.6 Illustration of our model for the lattice variation along Γ-M direction

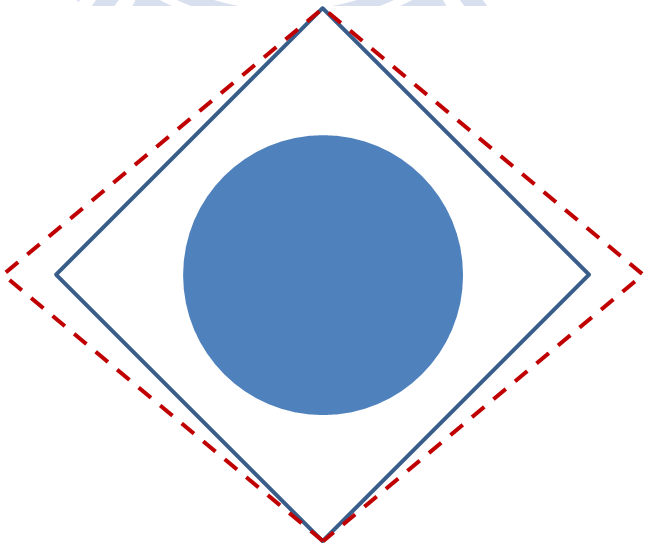

Figure 4-3.7 Illustration of a unit cell deviation of photonic crystal square-lattice rods structure with 20 % lattice extension along Γ-M direction

Figure 4-3.8 shows the Hz mode profiles for TE mode of photonic crystal rods laser with 705 nm lattice constant and r/a ratio of 0.37 in different lattice extension percentage of 0 %, 4 % and 10 % along Γ-M direction. Similar to lattice extension along Γ-X direction, the modes remain strongly localized in the rods while the lattice extended. It reveals that the photonic crystal square-lattice rods laser does not propagate in Γ-M direction.

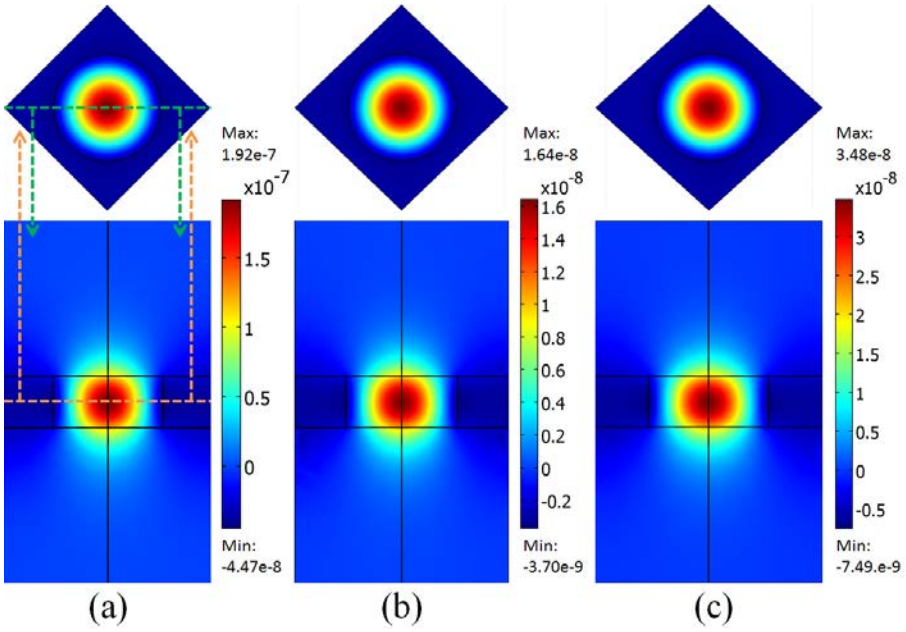

Figure 4-3.8 Mode profiles for TE mode in Hz field of photonic crystal square-lattice rods laser with 705 nm lattice constant in different lattice extension percentage along Γ-M direction. (a) Original un-extended square lattice (b) Lattice extension percentage of 4 % (c) Lattice extension percentage of 10 %

Comparing the experimental result to simulated result in 3-D FEM calculation, the red-shift behaviors of wavelength shown in Figure 4-3.9 are similar to each other. The simulated wavelength versus lattice extension percentage has a slop around 2.18 (nm/%) and the experimental wavelength versus lattice extension percentage has a slop around 1.72 (nm/%). However, the wavelength of experiment and simulation are not exactly the same but close. Both difference of wavelength peak and wavelength variation slop between experiment and simulation could be attributed to fabrication inaccuracy.

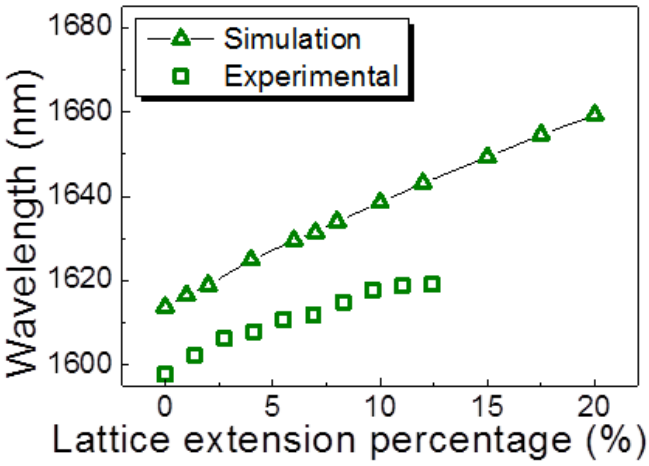

Figure 4-3.9 Comparison between experimental result and simulated result with extended lattice along Γ-M direction

4-4 Conclusions

In this chapter, we introduced a homemade extending stage to serve as a lattice extension platform. Both lattice extension along Γ-X and Γ-M direction were demonstrated and we find out that lattice extension along Γ-X direction has higher wavelength tunability of 2.97 (nm/%) than lattice extension along Γ-M direction of 1.62 (nm/%).Comparison between Γ-X and Γ-M direction is shown in Figure 4-4.1. Also 3-D FEM simulations were performed to confirm the experimental result.

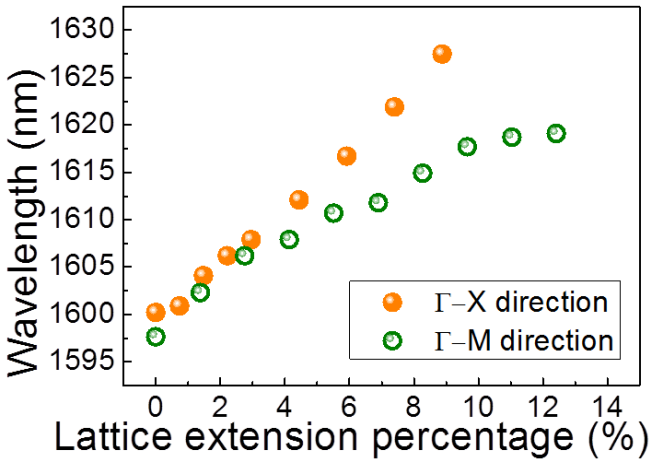

Figure 4-4.1 Comparison of wavelength tunability between lattice extension along Γ-X and Γ-M direction

Chapter 5

Summary and Future Works

In this thesis, the photonic crystal square-lattice rods laser was demonstrated on a flexible polymethylsiloxane (PDMS) substrate. With a homemade extending stage, the red-shift behavior was observed in this single mode laser. The tuning ability can reach up to around 3 nm in the lattice extension percentage of 1 %. Simulations with 2-D plane-wave-expansion method (PWE) and 3-D finite-element method (FEM) are performed to understand the lasing characterizations.

With our well-settled fabrication processes, the photonic crystal square-lattice rods structure was fabricated on the InGaAsP membrane content 4 quantum wells designed for 1.55 um communication wavelength, and then bonded to the flexible PDMS substrate. The lasing mode in flat plane was observed with low threshold power and identified with 0.44 in normalized frequency of the corresponding band structure. One of advantages of the flexible laser is the fine-tuning of optical properties by manipulating its geometry. Therefore we introduced a homemade extending stage to serve as the tunable platform. Both the lattice extension along Γ-X and Γ-M direction are experimented. The tuning range can achieve 26.4 nm in 8.88 % lattice extension percentage along Γ-X direction and 21.45 nm in 12.42 % lattice extension percentage along Γ-M direction. The wavelength tunability of the flexible photonic crystal laser extended along Γ-X direction is approximately 2.97 (nm/%), which is good enough to act as a tunable laser light source.

With several advantages including a larger tuning range in wavelength, flexibility on a PDMS substrate, and compactness of photonic crystal structure, the flexible photonic crystal laser can be applied for the multi-wavelength tunable light source in the future photonic integrated circuits with compact size, low threshold, and high output power.

In the future, there are several deep topics would be continued in this project:

1. We will demonstrate photonic defect lasers on the flexible platform. The defect modes might have various mode distributions by point-shifting the lattice, and then some optical properties will be altered. Because our flexible platform can fine-tune the lattice easily, we can investigate the lasing performance with low-cost flexible system.
2. We will demonstrate the tunable index sensor with the photonic crystal rods structure.
3. We will demonstrate the micro-scale photonic integrated circuit on the flexible platform.

Reference

[1] J. W. S. Rayleigh, “On the remarkable phenomenon of crystalline reflexion described by Prof. Stokes," Philosophical Magazine (sec. 5) **26**, 256 (1888)

[2] E. Yablonovitch, “Inhibited Spontaneous Emission in Solid-State Physics and Electronics,” Phys. Rev. Lett. **58**, 2059 (1987)

[3] S. John, “Strong localization of photons in certain disordered dielectric superlattices” Phys. Rev. Lett. **58**, 2486 (1987)

[4] D. G. Lidzey, “Strong Optical Coupling in Organic Semiconductor Microcavities,” Thin Films and Nanostructures **31**, 355 (2003)

[5] J. D. Joannopoulos, J. N. Winn, and R. D. Meade, “Photonic crystals: molding the flow of light,” Princeton University Press, Princeton (1995)

[6] P.R. Berman, “Cavity quantum electrodynamics,” New York: Academy (1994)

[7] O. Painter, R. K. Lee, A. Scherer, A. Yariv, J. D. O'Brien, P. D. Dapkus, I. Kim, “Two-Dimensional Photonic Band-Gap Defect Mode Laser,” Science **284**, 1819 (1999)

[8] O. Painter and K. Srinivasan, “Polarization properties of dipolelike defect modes in photonic crystal nanocavities,” Opt. Lett. **27**, 339 (2002)

[9] S. Noda, M. Fujita and T. Asano, “Spontaneous-emission control by photonic crystal and nanocavities,” Nature Photonics **1**, 449 (2007)

[10] T. Baba, “Slow light in photonic crystals,” Nature Photonics **2**, 465 (2008)

[11] J. P. Dowling, M. Scalora, M. J. Bloemer, and C. M. Bowden, “The photonic band-edge laser: A new approach to gain enhancement,” J. Appl. Phys. **75**, 1896 (1994)

[12] M. Imada, S. Noda, A. Chutinan, T. Tokuda, M. Murata and G. Sasaki, “Coherent two-dimensional lasing action in surface-emitting laser with triangular-lattice photonic crystal structure,” Appl. Phys. Lett. **75**, 316 (1999)

[13] K. Srinivasan, P. E. Barclay, M. Borselli and O. Painter, “Optical-fiber-based measurement of an ultrasmall volume high-Q photonic crystal microcavity,” Phys. Rev. B **70**, 081306 (2004)

[14] B. S. Song, S. Noda, T. Asano and Y. Akahane, “Ultra-high-Q photonic double heterostructure nanocavity,” Nature Materials **4**, 207 (2005)

[15] P.B. Deotare, M. W. McCutcheon, I.W. Frank, M. Khan and M. Lončar, “High quality factor photonic crystal nanobeam cavities,” Appl. Phys. Lett. **94**, 121106 (2009)

[16] L. Ferrier, O. El Daif, X. Letartre, P. R. Romeo, C. Seassal, R. Mazurczyk and P. Viktorovitch, “Surface emitting microlaser based on 2D photonic crystal rod lattices,” Opt. Expr. **17**, 9780 (2009)

[17] J. H. Burroughes, D. D. C. Bradley, A. R. Brown, R. N. Marks, K. Mackay, R. H. Friend, P. L. Burns and A. B. Holmes, “Light-emitting diodes based on conjugated polymers,” Nature **347**, 539 (1990)

[18] Y. Shi, C. Zhang, H. Zhang, J. H. Bechtel, L. R. Dalton, B. H. Robinson, W. H. Steier, “Low (Sub-1-volt) halfwave voltage polymeric electro-optic modulators achieved by controlling chromophore shape,” Science **288**, 119 (2000)

[19] O. L. J. Pursiainen, J. J. Baumberg, K. Ryan, J. Bauer, H. Winkler,B. Viel and T. Ruhl, “Compact strain-sensitive flexible photonic crystals for sensors,” Appl. Phys. Lett. **87**, 101902 (2005)

[20] G. P. Crawford, “Flexible flat panel display technology,” John Wiley & Sons (2005)

[21] M. H. Shih, K. S. Hsu, W. Kuang, Y. C. Yang, S. K. Tsai, Y. C. Liu, Z. C. Chang, and M. C. Wu, “Compact optical curvature sensor with a flexible microdisk laser on a polymer substrate,” Opt. Lett. **34**, 2733 (2009)

[22] M. H. Shih, K. S. Hsu, Y. C. Wang, Y. C. Yang, S. K. Tsai, Y. C. Liu, Z. C. Chang and M. C. Wu, “Flexible compact microdisk lasers on a polydimethylsiloxane (PDMS) substrate,” Opt. Expr. **17**, 991 (2009)

[23] 徐功書, “Fabrication and characterization of the compact microdisk lasers on the flexible substrate,” Master thesis, NCTU (2009)

[24] 邱子庭, “Fabrication and characterization of the photonic crystal band-edge laser on a PDMS substrate,” Master thesis, NCTU (2011)

[25] K. Kobayashi and I. Mito, “Single frequency and tunable laser diodes,” IEEE J. Lightw. Technol. **6**, 1623 (1988)

[26] L. A. Coldren, G. A. Fish, Y. Akulova, J. S. Barton, L. Johansson, and C. W. Coldren, “Tunable semiconductor lasers: a tutorial,” IEEE J. Lightw. Technol. **22**, 193 (2004)

[27] K. J. Kim, J. W. Kim, M. C. Oh, Y. O. Noh and H. J. Lee, “Flexible polymer waveguide tunable lasers,” Opt. Expr. **18**, 8392 (2010)